International Journal of Thermofluids 19 (2023) 100392

Contents lists available at ScienceDirect

International Journal of Thermofluids

journal homepage: www.sciencedirect.com/journal/international-journal-of-thermofluids

Performance assessment of hybrid recuperative heat exchanger for diesel engine generated exhaust gas

George Onyango Orido [a,b,*], Erick Kiplangat Ronoh [a], Patrick Ochuodho Ajwang [a], Benson Baari Gathitu [a]

[a] Agricultural and Biosystems Engineering Department, Jomo Kenyatta University of Agriculture and Technology, Kenya
[b] Egerton University, Faculty of Engineering and Technology, Agricultural Engineering Department, Kenya

ARTICLE INFO

Keywords:
Hybrid recuperative heat exchanger
Exhaust gas energy
Solar-exhaust gas greenhouse dryer
Diesel engine

ABSTRACT

In this study, the use of supplemental heat energy from exhaust gas of a stationary diesel engine was assessed to explore a new method of drying black nightshade seeds in a solar-exhaust gas greenhouse dryer. The energy recovery potential of a hybrid recuperative heat exchanger (HRHE) was demonstrated with the objective of utilizing the recovered energy from an engine on milling operations to heat a fluid stream of drying air. The results show that 4.45 kW of thermal energy was available in exhaust gas of a diesel engine operated at 2500 rpm when mass flow rate was 45.07 kg/h at a temperature of 357.36 °C. The rate of heat utilized for solar-exhaust gas mode ranged from 40.49 to 685.94 $J/m^2.s$ and from 21.69 to 668.11 $J/m^2.s$ in exhaust gas mode of drying. The heat exchanger raised the dryer temperature by an average of 11.78 °C when temperature differences between inside and outside were compared in solar-exhaust gas mode of drying. The average hourly rise in temperature inside the dryer was 8.04 °C with a minimum rise of 3.7 °C and a maximum of 9.41 °C when exhaust gas was utilized to provide heat energy. The performance of the solar-exhaust gas greenhouse dryer improved when thermal energy was used as a supplement in drying and as a result the drying time for black nightshade seeds was significantly reduced from 11 h in solar mode to 10 h in solar-exhaust gas mode of drying. Moreover, the seeds were dried for 14 h when exhaust gas mode of drying was performed without utilizing solar energy. The percent internal uncertainty for experimental measurements of relative humidity (γ) was 4.1% and 17.5% for temperature (*T*) observations. The three proposed thermal models for temperatures and moisture evaporation performed better with low RMSEs in exhaust gas mode compared to the other modes of drying.

1. Introduction

In the agriculture sector, diesel engines are used for both mobile and stationary farm operations due to their improved specific power output, durability, fuel economy, and reliability. Early research conducted by Wang et al. [1] successfully applied energy from exhaust gas of a diesel engine to drive an adsorptive ice maker. A new concept based on heat pipe technology has been introduced to effectively harness waste heat generated in nuclear power reactors for sea water desalination [2] . Recent advances in waste heat recovery from engines have been documented by Wang et al. [3] with a proposal of a resorption system combined with an energy storage function to recover waste heat from vehicles. The authors analysed possible phase change materials (PCMs) for energy storage function with the consideration that the melting point of PCM should be lower than the exhaust gas temperature of 250 °C [3] . Heat-pipe based heat exchangers have been potentially applied in cooling data-centres with achievable energy savings of up to 75% [4] . In an analysis of the integration of a trigeneration scheme within a Natural Gas Processing Plant (NGPP) that uses waste heat from gas turbine exhaust gas, Popli et al. [5] found that the trigeneration system could recover 79.7 MW of gas turbine waste. In the steel industry, a flat heat pipe (FHP) heat exchanger has been used in recovery of residual heat to significantly reduce production costs and greenhouse gas emissions [6] . Alklaibi [7] has reported results indicating that for maximal efficiency, use of heat from a gas turbine exhaust gas and air bottoming exhaust air is best performed by an absorption system in a cogeneration plant. In the ceramics industry, Jouhara et al. [8] designed, manufactured, and installed a heat pipe heat exchanger (HPHE) system on a roller hearth kiln and managed to recover up to 100 kW at steady state without cross contamination or excess fouling. A comprehensive review of state-of-the-art applications, materials and performance of heat pipe

* Corresponding author.
E-mail address: george.orido@egerton.ac.ke (G.O. Orido).

https://doi.org/10.1016/j.ijft.2023.100392

Available online 7 June 2023

Nomenclature

$\dot{A}_{ex}$	Rate of available thermal energy in the exhaust gas (kW)
A_C	The cross-sectional area (m^2)
CN1 to CN6	Connectors numbered 1 to 6
CO	Carbon monoxide
CO_2	Carbon dioxide
C_P	Specific heat capacity at constant pressure (kJ/kg.°C)
C_{ex}	Specific heat capacity of exhaust gas (kJ/kg.°C)
$\dot{C}_{conv}$	Convection heat transfer rate in connectors (kW)
c_{conv}	Convection heat transfer coefficient in connectors (W/m^2.°C)
DES	Diesel engine speed (rpm)
D	Diameter (m)
HC	Hydrocarbons
H_2O	Water vapor
h	Specific enthalpy (kJ/kg)
h_{conv}	Convection heat transfer coefficient (W/m^2.°C)
k	Thermal conductivity (W/m.°C)
K	Discharge coefficient
L_C	Characteristic length (m)
MW	Mega Watt
$\dot{m}_{ex}$	Mass flow rate of exhaust gas (kg/h)
m_{ev}	Moisture evaporated (g)
N	Number of sets
N_0	Number of observations in each set
NOx	Nitrogen oxides
Nu	Nusselt number
Nu_{cn}	Nusselt number in connectors
Nu_{tb}	Nusselt number in tubes
P	Pressure (kN/m^2)
Pr	Prandtl number
PM	Particulate matter
$\dot{Q}_{conv}$	Convection heat transfer rate (kJ/h)
Q_{ex}	Volumetric flow rate (m^3/s)
Re	Reynolds number
Re_{cn}	Reynolds number in connectors
Re_{tb}	Reynolds number in tubes
rpm	Revolutions per minute
s	Specific entropy (kJ/kg.°C)
S_A	Surface area (m^2)
TB1 to TB6	Tubes numbered 1 to 6
T	Temperature (°C)
T_{amb}	Ambient temperature (°C)
T_{ex}	Exhaust gas temperature (°C)
T_s	Surface temperature (°C)
T_b	Black nightshade seeds temperature (°C)
T_r	Greenhouse dryer room air temperature (°C)
$\dot{T}_{conv}$	Convection heat transfer rate in tubes (kW)
t_{conv}	Convection heat transfer coefficient in tubes (W/m^2.°C)
ΔT_{ex}	Difference between measured exhaust gas and ambient temperatures (°C)
U'	Parameter for% internal uncertainty
V_{ex}	Average velocity of exhaust gas (m/s)
V_{cn}	Average velocity of exhaust gas in connectors (m/s)
V_{tb}	Average velocity of exhaust gas in tubes (m/s)
$X - \bar{X}$	Deviation of observation from mean

Greek letters

γ	Relative humidity
ζ	Greenhouse dryer room air temperature model parameter
μ	Dynamic viscosity ($N.s/m^2$)
ξ	Black nightshade seeds model parameter
ϖ	Random error parameter in black nightshade seeds model
ρ	Density (kg/m^3)
ϱ	Random error parameter in greenhouse dryer room air temperature model
σ	Standard deviation
Ω	Moisture evaporated model parameter

Subscripts

amb	Ambient
calc	Calculated
conv	Convection
crit	Critical
ex	Exhaust gas
expt	Experimental
pred	Predicted
sur	Surface

Abbreviation

AfDB	African Development Bank
BMEP	Brake Mean Effective Pressure
EGR	Exhaust Gas Recirculation
HRHE	Hybrid Recuperative Heat Exchanger
JKUAT	Jomo Kenyatta University of Agriculture and Technology
K-INCUD	Khwisero Integrated Community Umbrella Development
MoEST	Ministry of Education Science and Technology
PCM	Phase Change Material
PPCI	Partially Premixed Compression Ignition
NGPP	Natural Gas Processing Plant
RMSE	Root Mean Squared Error
TIG	Tungsten Inert Gas
WLHP	Wraparound Loop Heat Pipe

devices has been documented by Jouhara et al. [9] and the popularity of heat pipes as passive heat transfer technologies due to their high efficiency was reported. In a study by Liu et al. [10] aimed at engine exhaust gas energy recovery through direct and indirect means, results have shown that direct recovery bottom cycle through secondary expansion suits diesel engines at full load with high boost pressure. Notwithstanding, indirect recovery bottom cycles have a substantial applied range with their exhaust gas energy recovery potential higher compared to direct recovery means. Jouhara et al. [11] have reviewed waste heat recovery techniques such as direct contact condensation recovery, indirect contact condensation recovery, transport membrane condensation and the use of units such as heat pumps, heat recovery steam generators (HRSGs), heat pipe systems, organic Rankine cycles, including the Kalina cycle, that recover and exchange waste heat with potential energy content. Organic Rankine cycle power units have been recently used in the recovery of waste heat from proton exchange membrane fuel cell system in a study by Wilberforce and Muhammad [12] while Mahmoud et al. [13] investigated of a ground-cooled organic Rankine cycle for waste heat recovery from a diesel generator. The composition of diesel engine exhaust gas includes carbon monoxide (CO), hydrocarbons (HC), nitrogen oxides (NOx), and particulate matter (PM). Jouhara and Olabi [14] have advocated the need for solutions to reduce the production of greenhouse gasses and also lower the level of global warming through development and utilization of waste heat technologies. An experimental study by Zhang et al. [15] was conducted to further improve understanding of injection strategies on engine performance and NOx emission of 17.4 g/kWh was reported. In a similar study by Zheng et al. [16] , it was reported that ethanol shows potential

for reducing NOx emissions to less than 1.5 g/kWh. In comparison to composition of air, exhaust gas from a diesel engine have higher concentrations of water vapor (H_2O) and carbon dioxide (CO_2) which are the main combustion products. By comparison, concentrations of pollutants from a diesel engine are small, therefore, to determine physical properties of diesel exhaust gas, they are neglected. Zhang et al. [17] have directly supplied compressed air to a stationary diesel engine to investigate soot emissions which increased with increasing intake pressure and decreased with increasing intake temperature. The authors compared thermal efficiency of supplied compressed air to a diesel engine against a hybrid system consisting of compressed air engine and a baseline diesel engine. In another study by Zheng et al. [18] , combustion and emissions of a single-cylinder diesel engine have been investigated under high exhaust gas recirculation of 46% with two-stage injection strategies (pilot-main and main-post). In their conclusion, the authors reported that NOx emissions decrease first and then increased with increasing pilot-main interval. However, carbon monoxide increased with increasing pilot-main interval while NOx emissions decreased with increasing main-post interval. De Poures et al. [19] have attempted to minimize emissions of a single-cylinder diesel engine by using waste cooking oil and C8 oxygenate blends. Pan et al. [20] have established that smoke and nitrogen oxide could be minimized simultaneously using exhaust gas recirculation. Dhahad et al. [21] have reported 4.3 g/kWh as the maximum CO level achieved at an engine speed of 1000 rpm and 1 bar engine load for ultra-low sulfur diesel use. At similar engine speed and pressure, 4.7 g/kWh of CO level was reported when diesel-water emulsion was used. Minimum CO levels were reported as 2.9 and 2.34 g/kWh at 2250 rpm and 625 bars for ultra-low sulfur diesel and diesel-water emulsion use, respectively [21] . Chaichan [22] used 85% bioethanol and 15% unleaded gasoline as E85-diesel blend in a partially premixed compression ignition (PPCI) engine and reported increased CO and HC concentrations. PPCI combustion caused significant improvement in NOx-PM trade-off and cooled exhaust gas recirculation (EGR) addition significantly expanded the engine torque range. Maize has been the main staple crop of Kenya for both urban and rural populations. According to De Groote and Kimenju [23] , Kenyan consumers strongly prefer white milled maize whose preparation for lunch and dinner is dished as *ugali* (a stiff, dryer preparation). Food security has depended on ensuring adequate supplies of maize to be milled by diesel operated engines that power *posho* mills in Kenya. These engines, mostly used in milling operations, lose 30% of their fuel energy through exhaust emissions in the form of heat to the environment. It has been reported that exhaust gas immediately leaving diesel engines can have temperatures as high as 450–600 °C [24] . There is a need, therefore, to develop strategies to recover exhaust gas heat energy from these stationary diesel engines on milling operations and the solution as provided in the current work is to structurally design heat exchangers to recover heat energy from exhaust gas generated by the engines. According to Tavousi et al. [25] , it is imperative to design efficient heat exchangers that are simpler, cheaper to manufacture, have higher rates of heat transfer, and low in pressure drop, to meet the growing need for more energy. In advanced systems wraparound loop heat pipes (WLHP) charged with R134a as the working fluid are used for heat energy recovery because of their overall effective thermal resistances which is as low as 0.048 °C/W [26] . Heat exchangers are classified according to the degree of surface compactness, heat transfer mechanisms, transfer processes, flow arrangements, construction features, and the number of fluids. An exploration and review by Jouhara et al. [11] revealed the operation and performance of commonly waste heat recovery technologies such as recuperators, regenerators, including furnace regenerators and rotary regenerators or heat wheels, passive air preheaters, regenerative and recuperative burners, plate heat exchangers and economizers and units such as waste heat boilers and run around coil (RAC). In the present work, a HRHE was developed to recover exhaust gas heat energy from a stationary diesel engine and the energy was utilized as a supplement in a solar greenhouse dryer when radiation was low and at night. Uses of new emerging technologies for direct heat to power conversion such as thermoelectric, piezoelectric, thermionic, and thermo photo voltaic (TPV) power generation techniques have been discussed in detail by Jouhara et al. [11] . Nevertheless, thermal energy storage and management problems were encountered in the current study and proposed solutions lie in the design of solar harvester systems, use of phase change materials (PCM), and mechanisms of storage (sensible heat, latent heat, and sorption heat) as reported by a number of authors [27–30] . Different types of PCM such as wax, salt hydrate and salt hydrate mixtures have been investigated for their heat capacity and results showed that wax was the most suitable PCM [31] . In the present study, the floor of the greenhouse dryer was painted black to optimize the absorption of solar rays because according to Murr et al. [32] , for black bodies the absorptivity and emissivity are approximately equal and close to one. Kiburi et al. [33] have demonstrated that flue gas from biomass can be utilized as a supplemental heat source in a greenhouse dryer to increase annual revenue by 147.59% for the solar mode only. Kanali et al. [34] have developed and piloted a multipurpose solar-biomass dryer with the Khwisero Integrated Community Umbrella Development (K-INCUD) group, in Kakamega County, Kenya. Previous studies by Kiburi et al. [33] , Kanali et al. [34] , and Ndirangu et al. [35] on solar-biomass dryers have recommended more tests on the dryers performance and introduction of supplemental energy for faster drying. As a new contribution from the current work, a HRHE was introduced as a strategy to recover exhaust gas heat energy from a stationary diesel engine to heat drying air in a modified solar-exhaust gas greenhouse dryer. The expected output from this study was quicker and continuous drying of black nightshade seeds in a solar-exhaust gas greenhouse dryer when radiation was low during the day and during nighttime when there was no solar radiation. The benefit of the heat exchanger in the whole system was to transfer heat energy from exhaust gas released by a diesel engine to the greenhouse dryer inside environment for drying purposes. As a justification, the present work was chosen to promote the conservation of black nightshade crop through seeds drying to recommended conditions to improve germination and subsequently to preserve the biodiversity of the beneficial vegetable crop—black nightshade has been reported to have larvicidal activity against *stegomyia aegypti*, a common vector of dengue fever—according to Chowdhury et al. [36] . The main objective of this work was to recover heat energy from exhaust gas of a stationary diesel engine doing milling operations and then to utilize the energy to heat a fluid stream of drying air in a solar-exhaust gas greenhouse dryer for black nightshade seeds.

2. Materials and methods

2.1. Description of study site

Field experiments were set up at the Department of Agricultural and Biosystems Engineering, Jomo Kenyatta University of Agriculture and Technology (JKUAT), Kenya. The latitude and longitude angles of the University are 1º5′ 20.8″S and 37º0′ 30″E, while the altitude is 1527 m above the sea level. The mean annual temperature is 19.85 °C with a mean annual maximum temperature of 24.91 °C and a mean annual minimum temperature of 14.79 °C. The relative humidities range from 15–80%. The climate for the study site is considered warm and temperate with an annual bimodal rainfall of 1014 mm characterized by cold rainy seasons occurring from April to August and October to December each year.

2.2. Experimental set up

The solar-exhaust gas greenhouse dryer used in this study is shown in Fig. 1 (outside view). The measurements of the dryer were 8 m long, 4 m wide, and 2.6 m high. Fig. 2. shows the hybrid recuperative heat exchanger designed and developed to harvest exhaust gas heat energy

Fig. 1. Outside view of the solar-exhaust gas greenhouse dryer.

Fig. 2. Recuperative heat exchanger in the solar-exhaust gas greenhouse dryer.

from a diesel engine inside the dryer. A labeled portion of the heat exchanger is shown in Fig. 3.. Four drying trays, two on the right and two on the left were fabricated inside the dryer to measure 6 m long by 1 m wide with a spacing of 0.3 m between the two levels of drying. The heat exchanger was placed below the drying trays and food-grade plastic mesh screen held the drying products in position during the thin layer drying experiment as presented in Fig. 4.

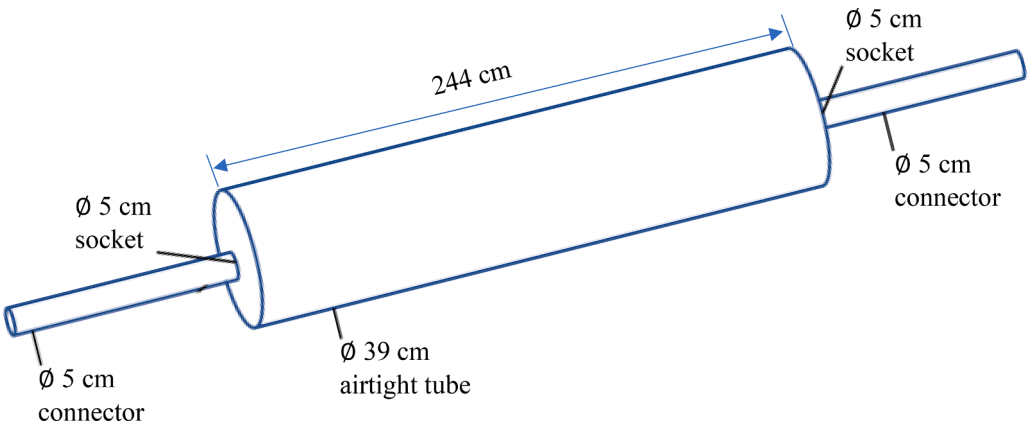

Fig. 3. Schematic diagram of hybrid recuperative heat exchanger portion.

Fig. 4. Thin layer drying of black nightshade seeds on a drying tray.

2.3. Instrumentation and data acquisition

To study the variation of temperature and relative humidity profiles inside and outside the solar-exhaust gas greenhouse dryer, twenty-six (AM2301A, China) temperature and relative humidity composite sensors with calibrated digital signal output were used. Twenty-four of the sensors were placed at the desired locations inside the dryer while one RH sensor and another temperature sensor were placed outside the dryer. Surface temperatures of connectors and tubes of the heat exchanger were measured using twelve (DS18B20, China) programmable resolution 1-wire digital thermometers with operating temperature range of −55 °C to +125 °C (± 0.1). The sensors (AM2301A, China), and (DS18B20, China), were programmed to record data in a microcontroller (ATmega2560, Italy). The Arduino Mega microcontroller was equipped with a 2 GB microSD card for data storage of the experiments.

2.4. Heat exchanger development

The research machine in this work was a naturally aspirated diesel engine whose name is R175A. This engine was used to power a stationary milling machine on the farm. The basic parameters of the R175A engine are listed in Table 1. To provide boundary conditions for performance calculation, a steady state heat balance was carried out in the thermofluids laboratory at JKUAT on a test engine shown in Fig. 5.. The engine had similar specifications to the R175A and the experimental data under the benchmark operating condition point of 2500 rpm and mean effective pressure of 576 kN/m^2 were obtained. Previously, Zhang et al. [15] selected an operating condition of 1.5 MPa BMEP and 1500 rpm engine speed when conducting experiments of injection strategies on engine performance. In the current study, the single cylinder compression ignition engine running on diesel fuel was tested for engine speed, *DES* (rpm); exhaust gas temperature, T_{ex} (°C); exhaust gas mass

Table 1
Basic parameters of diesel engine.

Item	Content
IC engine type	Single cylinder
Bore (mm)	75
Stroke (mm)	80
Displacement (L)	0.353
Compression ratio	21:1
Specific fuel consumption (kg/kWh)	0.2802
Maximum Speed (rpm)	2500
Mean effective pressure (kN/m^2)	576
Valve clearance (mm)	Inlet valve 0.15–0.25; Exhaust valve 0.25–0.35
Fuel tank capacity (L)	4
Rated power (kW)	4.4
Injection pressure (kN/m^2)	$1.42 \times 10^4 \pm 5 \times 10^2$
Cooling mode	Water cooled
Intake mode	Naturally aspirated

flow rate, $\dot{m}_{ex}$ (kg/h); exhaust gas volumetric flow rate, Q_{ex} (m^3/s); exhaust gas velocity in connectors, V_{cn} (m/s); and exhaust gas velocity in tubes, V_{tb} (m/s). Five other exhaust gas properties corresponding to engine speed were computed based on relevant fluid and thermal equations for heat transfer mechanism.

Some of the assumptions made when diesel exhaust gas was used as a working fluid in the heat exchanger included: the existence of steady operating conditions; negligible potential energy; and use of air properties for exhaust gas. The heat exchanger was named HRHE based on the construction and the counterflow configuration. It has separate flow paths for exhaust gas and drying air. The two fluids flow simultaneously through the heat exchanger as heat is exchanged across the wall separating the flow paths. In the solar-exhaust gas greenhouse dryer environment, the inlet air from outside was allowed to flow from one direction, pick up moisture from the drying product and exit in an opposite direction. The heat exchanger ran across the greenhouse dryer environment to entirely cover it. Exhaust gas was channeled to flow through the tubular heat exchanger and allowed to exit at one end. The greenhouse dryer environment was heated through convective heat transfer from exhaust gas, through the heat exchanger surface and to the dryer environment. Table 2, adapted from Perry and Green [37] shows the physical properties of air at a pressure of 101.13 kPa.

To assess exhaust gas thermal energy available in a diesel engine in the thermofluids laboratory, modern convenient emission measurement system research tools were used. Temperature sensors of type K thermocouples (RTD type-PT100) capable of transmitting temperature data in the range of 0–1200 °C were used with a software for engine performance analysis as presented in Fig. 6. Besides temperature measurements, exhaust gas mass flow rate was measured using a pitot tube flow sensor (mass flow rate meter) which was part of a portable exhaust gas analyzer. The mass flow rate of the exhaust gas was computed based on Bernoulli and flow continuity equations using the pitot tube as indicated in Eq. (1). Large changes in pressure differences reflected small changes in the flow because of the square root relationship, therefore, four pressure difference sensors were incorporated with ranges that span more than two orders of magnitude to overcome the problem of a limited dynamic range associated with flow meters based on differential pressure.

$$\dot{m}_{ex} = K(Re) \times A\sqrt{\rho_{ex}(P_{HIGH} - P_{LOW})} \tag{1}$$

In Eq. (1), $\dot{m}_{ex}$ is exhaust gas mass flow rate, $K(Re)$ is discharge coefficient for flow tube assembly as a function of Reynolds number, A is physical cross-sectional area of flow tube assembly, ρ_{ex} is density of exhaust gas, and $(P_{HIGH} - P_{LOW})$ is differential pressure. To determine the available energy in the exhaust gas, the relationship presented in Eq. (2) was used.

$$\dot{A}_{ex} = \dot{m}_{ex} C_{ex} \Delta T_{ex} \tag{2}$$

Table 2
Physical properties of air ($P = 101.13$ kPa) [37] .

T	ρ	h	s	C_P	μ	k
-13.15	1.340	260.0	6.727	1.006	1.65×10^{-5}	0.0231
6.85	1.245	280.2	6.802	1.006	1.75×10^{-5}	0.0247
26.85	1.161	300.3	6.871	1.007	1.85×10^{-5}	0.0263
76.85	0.995	350.7	7.026	1.009	2.08×10^{-5}	0.0301
126.85	0.871	401.2	7.161	1.014	2.30×10^{-5}	0.0336
176.85	0.774	452.1	7.282	1.021	2.51×10^{-5}	0.0371
226.85	0.696	503.4	7.389	1.030	2.70×10^{-5}	0.0404
326.85	0.580	607.5	7.579	1.051	3.06×10^{-5}	0.0466
526.85	0.435	822.5	7.888	1.099	3.70×10^{-5}	0.0577
726.85	0.348	1046.8	8.138	1.141	4.24×10^{-5}	0.0681
926.85	0.290	1278	8.349	1.175	4.73×10^{-5}	0.0783
1126.85	0.249	1515	8.531	1.207	5.27×10^{-5}	0.0927

Fig. 5. Research engine test set up in thermofluids laboratory at JKUAT.

Fig. 6. Location of thermocouple temperature sensors for exhaust gas.

In Eq. (2), $\dot{A}_{ex}$ is available thermal energy in the exhaust gas, $\dot{m}_{ex}$ is mass flow rate of exhaust gas, C_{ex} is specific heat capacity of exhaust gas, and ΔT_{ex} is change in temperature of exhaust gas in comparison with the ambient temperature. For calculations of the available exhaust gas thermal energy, the specific heat capacity of exhaust gas was adopted as 1.0683 kJ/kg. °C an average value of the specific heat capacities of air, at constant pressure, for all the temperature ranges in Table 2. The need to recover energy from exhaust gas led to the conceptualization of a heat exchanger. Heat transfer in the separating wall of the heat exchanger was evaluated based on the analysis of the non-dimensional Nusselt number presented in Eq. (3) and Eq. (4). The working fluid inside the heat exchanger tube was exhaust gas from a diesel engine. The temperature difference between diesel engine exhaust gas and the wall surface of the heat exchanger was large. Consequently, the Sieder and Tate equation was used to evaluate Nusselt number for turbulent flow in connectors of the heat exchanger as expressed in Eq. (4). For the fully developed laminar flow in airtight cylindrical tubes of the heat exchanger where Reynolds number was less than 2000, Nusselt number was used as 3.66.

$$Nu = \frac{h_{conv} \cdot L_C}{k} \tag{3}$$

$$Nu = 0.027 \cdot Re^{0.8} \cdot Pr^{\frac{1}{3}} \cdot \left(\frac{\mu_{ex}}{\mu_{sur}}\right)^{0.14} \tag{4}$$

In Eq. (3), Nu is Nusselt number, h_{conv} is convection heat transfer coefficient, L_C is characteristic length and k is thermal conductivity. In Eq. (4), Nu is Nusselt number, Re is dimensionless Reynolds number, Pr is Prandtl number, μ_{ex} is dynamic viscosity of exhaust gas, μ_{sur} is dynamic viscosity of air at the surface of the heat exchanger wall material. Prandtl number was adapted from Rapp [38] and used as 0.72. The dynamic viscosity of air at the surface of the heat exchanger wall material was used as 1.85×10^{-5} N.s/m^2. The average velocity of exhaust gas as it flows through the connectors and tube was determined from Eq. (5).

$$V_{ex} = \frac{\dot{m}_{ex}}{\rho_{ex} \cdot A_C} \tag{5}$$

In Eq. (5), V_{ex} is average velocity of exhaust gas, $\dot{m}_{ex}$ is mass flow rate of exhaust gas, ρ_{ex} is exhaust gas density, and A_C is cross-sectional area through which exhaust gas flows. For computation of the average velocities of exhaust gas through connectors and airtight tubes of the heat exchanger, density of exhaust gas was adopted as 0.7487 kg/m^3, an average value of the densities of air at constant pressure. To determine whether diesel engine exhaust gas was in laminar or turbulent flow, Reynolds number was used as defined in Eq. (6).

$$Re = \frac{\rho_{ex} \cdot V_{ex} \cdot D}{\mu_{ex}} \tag{6}$$

In Eq. (6), Re is dimensionless Reynolds number, ρ_{ex} is diesel engine exhaust gas density, V_{ex} is average velocity of exhaust gas, D is diameter of connector or airtight cylindrical tube, and μ_{ex} is dynamic viscosity of exhaust gas. Classification of diesel engine exhaust gas flow through the heat exchanger was done according to Menon [39] where three main flow regimes have been reported as laminar flow with Reynolds number less than 2000, critical flow with Reynolds number greater than 2000 but less than 4000 and turbulent flow with Reynolds number greater than 4000. For calculations of Reynolds number, the dynamic viscosity of exhaust gas was adopted as 2.987×10^{-5} N.s/m^2 an average value of the dynamic viscosities of air, at constant pressure. The flow of exhaust gas through the heat exchanger was based on forced convection, such that a motion was generated by the action of a running diesel engine. The equation for the rate of convection heat transfer to the surface of the heat exchanger is given in Eq. (7).

$$\dot{Q}_{conv} = h_{conv} S_A (T_{ex} - T_s) \tag{7}$$

In Eq. (7), $\dot{Q}_{conv}$ is convection heat transfer rate, h_{conv} is convection heat transfer coefficient, S_A is surface area, T_s is surface temperature, and T_{ex} is exhaust gas temperature. This study introduced galvanized iron plates, sockets, unions, and connectors as the chosen materials of fabrication for the heat exchanger because of their availability, affordability, good ductility, and weldability—galvanized iron is ideal for metal fabrication and welding using tungsten inert gas (TIG) welding technique. The properties of galvanized iron that makes it suitable for this work are listed in Table 3.

The heat exchanger was designed to have circular surfaces on both front and back faces. Rolled plates were used to form cylindrical portions. The geometry of the heat exchanger was considered cylindrical with straight horizontal portions to allow for effective use of available sizes of galvanized iron materials. In the design, back pressure on exhaust system was considered. It was necessary to periodically lower and increase back pressure interchangeably to achieve the right amount

Table 3
Suitability of galvanized iron as fabricating material.

Property	Value
Specific heat capacity (kJ/kg.°C)	0.4605
Thermal conductivity (W/m.°C)	59
Melting point (°C)	1536.85
Density kg/m^3	7849
Thickness (mm)	1.6

and allow expulsion of exhaust gas from manifold. A galvanized iron pipe connector of 5 cm diameter [40,41] was connected to the diesel engine exhaust manifold to lower back pressure and allow exhaust gas to leave the engine. The length of the first connector, CN1, was guided by proximity of exhaust manifold to first tube, TB1, and width of dryer. The engine was operated at optimal speed, surface temperature of connector was measured, and velocity of exhaust gas was determined. Temperature of exhaust gas leaving a connector was measured and compared to ambient temperature with the objective to obtain an exit exhaust gas temperature desired at ± 1–2 °C above ambient temperature. Tubular part of the heat exchanger was made larger in diameter (39 cm) as compared to a connector's (5 cm) to create the circular geometry which allowed more flow of the working fluid thereby increasing retention time and total heat transfer as shown in Fig. 7. The diameter of tube was guided by height between floor and lower drying tray of dryer. To further lower back pressure, TB1 was introduced and connected as part of heat exchanger. Repeatedly, surface temperature, exhaust gas velocity and temperature at exit of tube were measured and recorded. A series of connectors (CN1-CN6), designed to increase back pressure, and tubes (TB1-TB6) designed to reduce back pressure formed the heat exchanger. They were developed and introduced in the dryer. Temperature inside the dryer was measured and compared to those of outside environment as a measure of performance and benefit of HRHE.

2.5. Thermal modeling and internal uncertainty analysis

The software R, version 4.1.3 [42] was used to develop simulation models from experimental data for prediction of black nightshade seeds temperature (T_b), greenhouse dryer room air temperature (T_r), and moisture evaporated (m_{ev}) from black nightshade seeds as given in Eqs. (8), (9) and (10), respectively.

$$T_{b-pred} = \xi_0 + \xi_1 t + \xi_2 T_{b-expt} + \xi_3 t T_{b-expt} + \xi_4 t^2 + \xi_5 \left(T_{b-expt}\right)^2 + \varpi \tag{8}$$

$$T_{r-pred} = \zeta_0 + \zeta_1 t + \zeta_2 T_{r-expt} + \zeta_3 t T_{b-expt} + \zeta_4 t^2 + \zeta_5 \left(T_{r-expt}\right)^2 + \varrho \tag{9}$$

$$m_{ev-pred} = \Omega_0 (1 - \exp(-\Omega_1 t \Omega_2)) + \Omega_3 \left(1 - \exp\left(-\Omega_4 m_{ev-expt} \Omega_5\right)\right) \tag{10}$$

In Eqs. (8), (9) and (10) the model parameters ξ_0 to ξ_5, ζ_0 to ζ_5, Ω_0 to Ω_5, and the random error terms ϖ and ϱ were determined through iteration and model fitting to experimental data. Microsoft 365 Excel software was used as a computational and graphical tool. To validate the experimental error, the percent internal uncertainty was determined using Eq. (11) [43,44].

$$\%\ internal\ uncertainty = \left[\frac{U'}{mean\ total\ number\ of\ observations} \times 100\right] \tag{11}$$

The parameter (U') for% internal uncertainty evaluation is found as shown in Eq. (12).

$$U' = \frac{\sqrt{\sigma_1^2 + \sigma_2^2 + \ldots + \sigma_N^2}}{N} \tag{12}$$

The standard deviation (σ) is given as expressed in Eq. (13).

$$\sigma = \sqrt{\frac{\sum (X - \bar{X})^2}{N_O}} \tag{13}$$

In Eq. (12) and Eq. (13) $(X - \bar{X})$ is the deviation of observations from the mean, (N) is the number of sets, and (N_O) is the number of

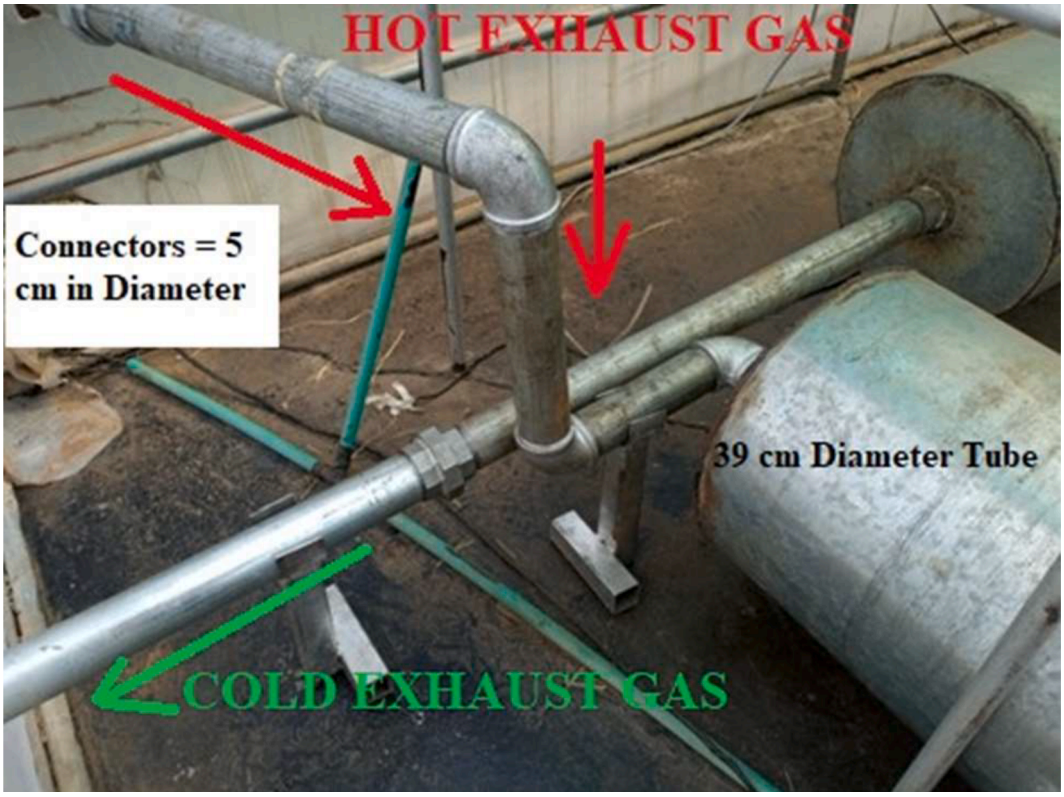

Fig. 7. Exhaust gas flow in connectors and tubes of hybrid recuperative heat exchanger.

observations in each set.

3. Results and discussion

3.1. Exhaust gas properties and heat exchanger dimensions

The percent internal uncertainty for experimental measurements of relative humidity (γ) was 4.1% and 17.5% for temperature (T) observations. Table 4 shows how exhaust gas properties correspond to engine speed. Exhaust gas temperature, mass and volumetric flow rates, velocities, Reynolds and Nusselt numbers, and available energy all increased with increasing engine speed. The maximum thermal energy available in the exhaust gas of the diesel engine used in this study was 4.45 kW when the engine was operated at 2500 rpm. In comparison, previous researchers have recovered up to 34 kW of waste heat when a diesel engine's driving load was 75 kW [45,46]. Table 5 is a summary of dimensional properties of connectors and tubes that make up the heat exchanger. In addition, mass of exhaust gas has been shown in connectors symbolized as CN1 to CN6 and tubes as TB1 to TB6. Mass of exhaust gas and volume increased with increasing distance from exhaust manifold. Table 6 presents the time taken in seconds by exhaust gas to fill connectors and tubes of the heat exchanger. Time reduced with increasing volumetric flow rate in connectors and tubes. A plot of exhaust gas heat energy variation with engine speed is shown in Fig. 8.. Increased engine speed results in increased heat energy in exhaust gas because of an increase in mass flow rate. At higher speeds of 2000 to 2500 rpm mass flow rates of exhaust gas had insignificant effect on temperatures. In the present study, it was important that the engine be operated at optimal speed (2500 rpm) as recommended by the manufacturer because low engine speeds and loads have been documented by Dhahad et al. [21] as conditions which increase CO and HC levels. In the previous study, a diesel engine was configured for experimental investigations and the results showed that NOx and smoke number reduced when diesel-water emulsion fuel was used compared to ultra-low sulfur diesel [21] .

The results of a one-way ANOVA performed using R software [42] indicated no significant difference between mass flow rates of exhaust gas for three engine speeds: 2000 rpm, 2250 rpm, and 2500 rpm, ($F_{calc,} = 2.767$, $F_{crit,\ 0.95} = 3.89$, $F_{crit,\ 0.99} = 6.93$ and p-value = 0.103). In previous work, Zhang et al. [17] reported maximum gross indicated thermal efficiency at intake pressure of 300 kPa and intake temperature of 300 K with 44.3%, which was 19.7% higher than the baseline diesel engine with 100 kPa intake pressure and 303 K intake temperature. Moreover, the authors reported 6.64% higher overall efficiency when using compressed air compared to hybrid system. The average velocity of exhaust gas was higher in connectors than in tubes of heat exchanger because average velocity, in either case, is inversely proportional to the cross-sectional area through which flow of exhaust gas takes place. Connectors were 5 cm and tubes were 39 cm in diameter. The exhaust gas mass flow rate of 45.07 kg/h resulted in the highest velocity. A flow rate of 11.32 kg/h resulted in the lowest velocity as presented in Fig. 9.

In Table 4 critical flows of exhaust gas at mass flow rates of 11.32 and 12.87 kg/h were observed at Reynolds numbers of 2681 and 3048, respectively in connectors. Exhaust gas mass flow rates between 29.79 and 45.07 kg/h resulted in Reynolds number greater than 4000 in connectors. In tubes, the flow regime was laminar at Reynolds number less than 2000. Convection heat transfer coefficients ranged from 13 to 40 W/m^2. °C in connectors. These results agree with those reported by Kosky et al. [47] in the forced convection range for air (10 to 500 W/m^2. °C). Convective heat transfer coefficients increased with increasing Reynolds number in the case of connectors. This observation was similarly reported by Jouhara et al. [48] when increased Reynolds number of flow led to high heat transfer coefficients and lower thermal forced convection resistances.

3.2. Heat exchanger performance in solar-exhaust gas mode of drying

To analyze heat exchanger performance, Fig. 10 illustrates the comparison of drying time between solar and solar-exhaust gas modes of drying. The heat exchanger provided additional heat energy for quicker drying of black nightshade seeds. Drying took 10 h in solar-exhaust gas mode as compared to 11 h in solar mode of drying. Temperature and relative humidity variations during the experiment are presented in Fig. 11. In solar mode of drying, temperature inside the dryer ranged between 14.82 and 58.46 °C. In solar-exhaust gas mode of drying, the range was observed from 34.49 to 61.97 °C. The heat exchanger raised the dryer temperature by an average of 11.78 °C when temperature differences between inside and outside were compared in solar-exhaust gas mode of drying. In Fig. 11, the lowest temperature difference between inside and outside the dryer, was observed on the 4th hour of drying as 4.28 °C. The highest temperature difference of 21.25 °C was observed on the 2nd and 3rd hours of drying. In summary, Temperatures inside the dryer were higher than the corresponding outside temperatures throughout the drying period because the cover material used in the dryer harnessed solar energy to raise the temperature while at the same time heat energy recovered from exhaust gas of a diesel engine kept the temperatures high. Inside relative humidity was low as compared to the outside relative humidity for the first four hours of dying. The combination of high temperature and low relative humidity in a dryer increased the ability of drying air to carry away moisture.

Table 7 is a summary of experimental and predicted results of changes in evaporated moisture, greenhouse dryer room air temperature, black nightshade seeds temperature, and air relative humidity in solar-exhaust gas mode of drying.

The results of moisture evaporated (experimental and predicted) and relative humidity are plotted in Fig. 12 from which the model's performance based on RMSE was found as 0.5186. The rate of heat utilized for solar-exhaust gas mode of drying ranged from 40.49 to 685.94 J/m^2. s and peaked after 8 h of drying when convective heat transfer coefficient for black nightshade seeds was 2.55 W/m^2. °C and evaporative heat transfer coefficient was 18.29 W/m^2. °C. Moisture evaporated and relative humidity decreased with increasing drying time. Residual plots of predicted moisture evaporated are illustrated in Fig. 13 with five positive data points, and six clustered on residual equal to zero line. A correlation coefficient of one was obtained for predicted versus experimental moisture evaporated as shown in Fig. 14. From a two-tailed t-test

Table 4
Exhaust gas properties corresponding to engine speed.

DES (rpm)	T_{ex} (°C)	$\dot{m}_{ex}$ (kg/h)	Q_{ex} (m^3/s)	V_{cn} (m/s)	V_{tb} (m/s)	Re_{cn}	Re_{tb}	Nu_{cn}	Nu_{tb}	$\dot{A}_{ex}$ (kW)	c_{conv} (W/m^2. °C)	$\dot{C}_{conv}$ (kW)	t_{conv} (W/m^2. °C)	$\dot{T}_{conv}$ (kW)
750	197.19	11.32	0.0042	2.14	0.035	2681	344	14	3.66	0.58	13	0.10	0.44	0.20
1000	213.47	12.87	0.0048	2.43	0.040	3048	391	16	3.66	0.72	15	0.12	0.44	0.22
1250	238.54	29.79	0.0111	5.63	0.093	7055	905	31	3.66	1.89	29	0.27	0.44	0.26
1500	325.07	33.21	0.0123	6.28	0.103	7865	1008	34	3.66	2.96	32	0.42	0.44	0.37
1750	352.94	37.65	0.0140	7.11	0.117	8917	1143	37	3.66	3.66	35	0.51	0.44	0.40
2000	359.82	41.46	0.0154	7.83	0.129	9819	1259	40	3.66	4.12	38	0.56	0.44	0.41
2250	356.98	42.53	0.0158	8.04	0.132	10,073	1291	41	3.66	4.19	38	0.57	0.44	0.41
2500	357.36	45.07	0.0167	8.52	0.140	10,674	1368	43	3.66	4.45	40	0.60	0.44	0.41

Table 5
Dimensional properties of connectors, tubes, and exhaust gas mass.

Property	CN1	CN2	CN3	CN4	CN5	CN6	TB1	TB2	TB3	TB4	TB5	TB6
Distance from exhaust manifold (m)	2.1	5.0	7.8	10.7	13.5	16.3	4.6	7.4	10.3	13.1	15.9	18.8
Volume (m^3)	0.004	0.3	0.6	0.9	1.2	1.5	0.3	0.6	0.9	1.2	1.5	1.8
Mass of exhaust gas (kg)	0.003	0.2	0.4	0.7	0.9	1.1	0.2	0.4	0.7	0.9	1.1	1.3

Table 6
Time (seconds) taken to fill connectors and tubes of heat exchanger.

(m^3/s)	CN1	CN2	CN3	CN4	CN5	CN6	TB1	TB2	TB3	TB4	TB5	TB6
0.0042	1.00	71	140	210	279	349	70	140	210	279	349	418
0.0048	0.88	62	123	185	246	307	62	123	184	246	307	368
0.0111	0.38	27	53	80	106	133	27	53	80	106	133	159
0.0123	0.34	24	48	72	95	119	24	48	71	95	119	143
0.0140	0.30	21	42	63	84	105	21	42	63	84	105	126
0.0154	0.27	19	38	57	76	95	19	38	57	76	95	114
0.0158	0.27	19	37	56	74	93	19	37	56	74	93	111
0.0167	0.25	18	35	53	70	88	18	35	53	70	88	105

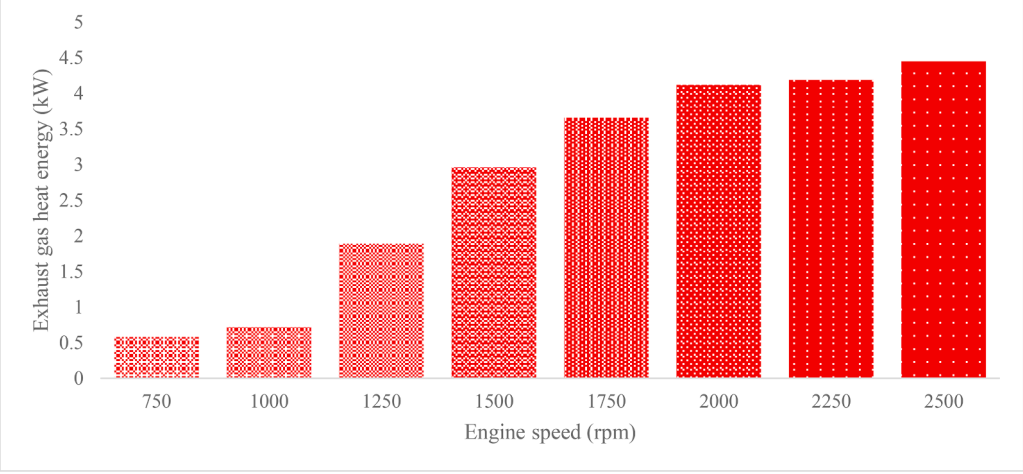

Fig. 8. Variation of exhaust gas heat energy with engine speed.

of two samples while assuming equal variances at 0.05 level of significance, experimental moisture evaporated data had a mean of 3.93 g when the predicted had a mean of 3.66 g ($t_{calc} = 0.9106$, $t_{crit} = 2.1001$). Thus, there was enough evidence to retain the null hypotheses that there is no difference in the means between predicted and experimental observations of moisture evaporated and it was concluded with 95% confidence that the model is useful in predicting moisture evaporated from black nightshade seeds. The solver converged to a solution after all the constraints were satisfied with iterations performed for which the objective function (minimum sums of squares of residuals) did not move significantly. From the iterations performed, the model parameters Ω_0, Ω_1, Ω_2, Ω_3, Ω_4, and Ω_5 were quantified for solar-exhaust gas mode of drying.

The experimental and predicted black nightshade seeds temperatures against drying time are plotted in Fig. 15 from which the results of the model's performance based on RMSE was found as 1.9524. The plot shows that there is an increasing nonlinear relationship between drying time and black nightshade seeds temperature for the first eight hours of drying and thereafter, a decreasing nonlinear relationship is observed for the rest of the drying period. The corresponding residual versus fits plot for the data set with black nightshade seeds temperature as the response and drying time as the predictor is shown in Fig. 16. The residual plots show nonlinearity and an indication of cyclic behavior. Fig. 17 is a goodness of fit plot of the predicted temperatures against experimental observations which show a correlation coefficient of 0.9947. The predicted black nightshade seeds temperature show agreement with experimental observations and from Fig. 16, none of the data points fell directly on the residual equal to zero line. The residuals depart from the zero line in a systematic manner with most of the data points concentrated between 45 and 60 °C and are positive for six values and negative for five values. From a two-tailed *t*-test of two samples while assuming equal variances at 0.05 level of significance, experimental black nightshade seeds temperature data had a mean of 53.48 °C when the predicted data had a mean of 53.03 °C ($t_{calc} = 0.9142$, $t_{crit} = 2.0860$). Thus, there was enough evidence to retain the null hypotheses that there is no difference in the means between predicted and experimental observations of black nightshade seeds temperatures and it was concluded with 95% confidence that the model is useful in predicting the temperature of the seeds. Model parameters ξ_0, ξ_1, and ξ_2 were quantified to show the main effects of screening and characterizing black nightshade seeds temperature prediction model. The model parameters ξ_3 quantified the interaction (cross product) term between drying time and experimental temperature data, ξ_4 quantified the first leading term with the second degree on drying time factor, ξ_5 quantified the second order term corresponding to black nightshade seeds experimental temperature and ϖ was the random error term that accounted for experimental error in the system.

Experimental and predicted greenhouse dryer room air temperatures against drying time are plotted in Fig. 18 from which the results of the model's performance based on RMSE was found as 1.7836. The plot

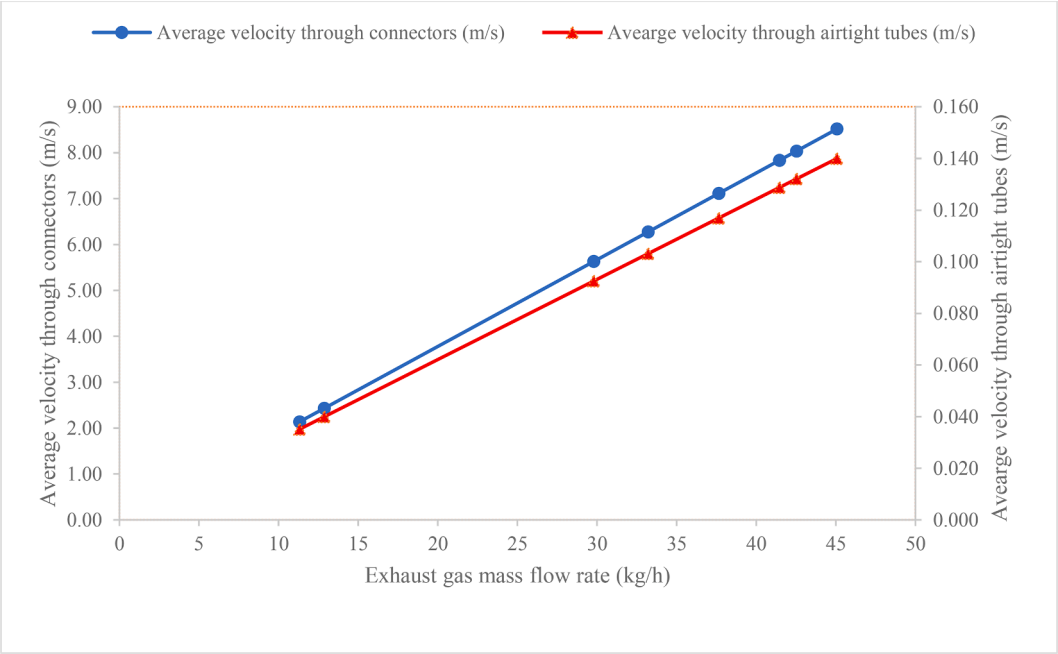

Fig. 9. Influence of exhaust gas mass flow rate on average velocity.

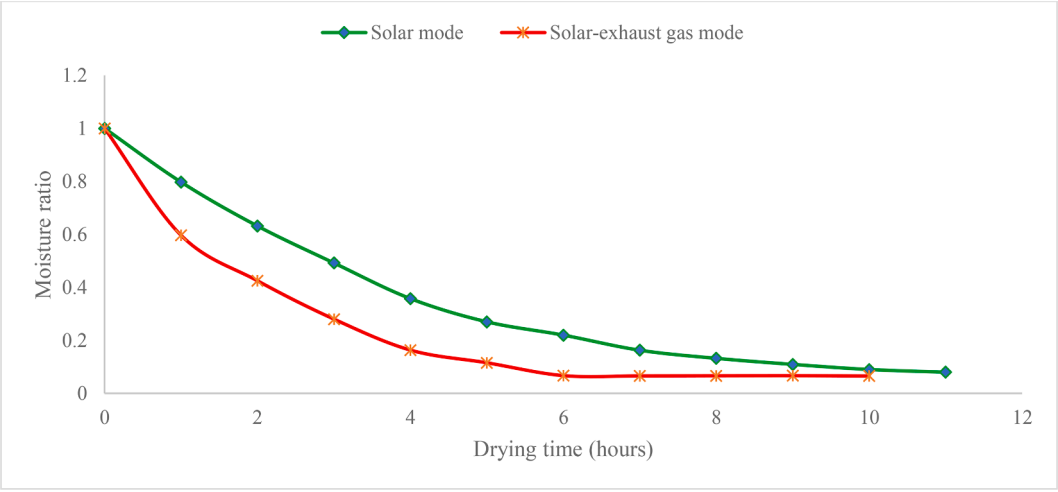

Fig. 10. Drying time comparison between solar and solar-exhaust gas modes of drying.

shows that there is an increasing nonlinear relationship between drying time and greenhouse dryer room air temperature for the first eight hours of drying and thereafter, a decreasing nonlinear relationship is observed for the rest of the drying period. The corresponding residual plot of greenhouse dryer room air predicted temperature is shown in Fig. 19. . The plot show nonlinearity and indication of cyclic behavior. Observations from Fig. 20 show a correlation coefficient of 0.9967. With reference to Fig. 19. , none of the data points fell directly on the residual equal to zero line. The residuals depart from the zero line in a systematic manner with most of the data points concentrated between 45 and 60 °C. Seven data points are positive while four are negative. A two-tailed *t*-test of two samples while assuming equal variances at 0.05 level of significance, show that experimental and predicted greenhouse dryer room air temperature data had means of 53.19 °C and 52.21 °C, respectively (t_{calc} = 0.8103, t_{crit} = 2.0860). Thus, there was enough evidence to retain the null hypotheses that there is no difference in the means between predicted and experimental observations of greenhouse dryer room air temperatures and it was concluded with 95% confidence that the model is useful in predicting room air temperature of the greenhouse dryer. Lad et al. [49] have successfully and efficiently maintained drying chamber temperature between 50 and 55 °C in an indirect solar dryer for food quality preservation when phase change material was used. Lad et al. [49] further reported average solar radiation of 660 W/m^2, average day temperature of 40 °C and average night temperatures of 30 °C which are consistent with the findings of the current study done in Kenya—a region with tropical climatic conditions characterized by high temperature and direct sunlight. From iterations, the model parameters ζ_0, ζ_1, and ζ_2 were quantified to show the main effects of screening and characterizing the greenhouse dryer room air temperature prediction model. The model parameters ζ_3 quantified the interaction (cross product) term between drying time and experimental temperature data, ζ_4 quantified the first leading term with the second degree on drying time factor, ζ_5 quantified the second order term corresponding to greenhouse dryer room air experimental temperature and ϱ was the random error term that accounted for the experimental error in the system.

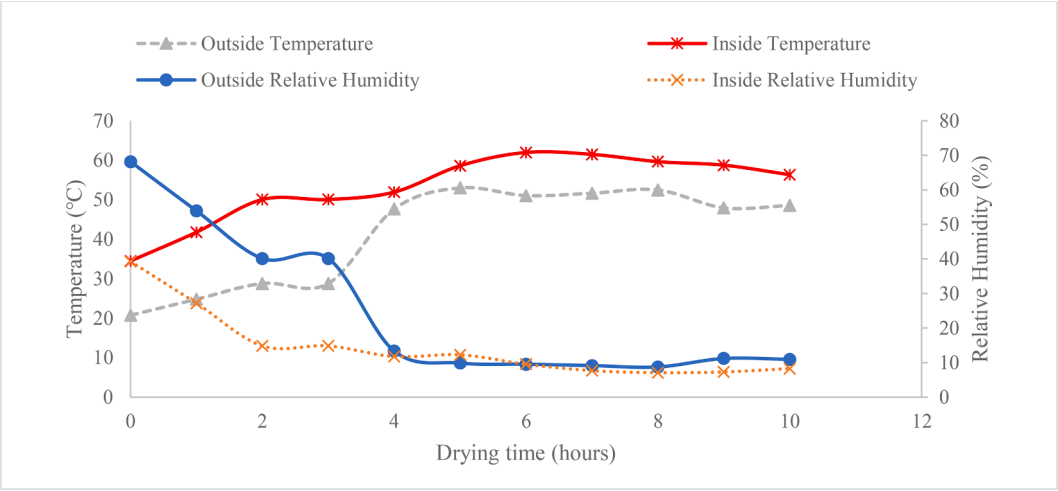

Fig. 11. Temperature and relative humidity variations in solar-exhaust gas mode of drying.

Table 7
Experimental and predicted data from forced convection solar-exhaust gas drying mode.

Drying Time (hours)	Experimental T_r (°C)	Predicted T_r (°C)	Experimental T_b (°C)	Predicted T_b (°C)	Experimental m_{ev} (g)	Predicted m_{ev} (g)	γ_v (%)
0	34.49	31.38	35.00	31.83	0	0	0.39
1	41.79	38.83	42.22	39.29	17.79	16.17	0.27
2	50.05	47.61	50.22	47.90	9.09	8.40	0.15
3	50.05	47.87	50.17	48.23	4.76	4.46	0.15
4	51.93	50.17	52.18	50.78	2.41	2.30	0.12
5	58.61	57.77	58.99	58.66	1.54	1.50	0.12
6	61.97	61.89	62.10	62.65	0.84	0.85	0.10
7	61.49	61.76	61.95	63.04	0.78	0.79	0.08
8	59.64	60.12	59.84	61.25	0.74	0.76	0.07
9	58.75	59.58	59.02	60.93	0.70	0.72	0.07
10	56.34	57.38	56.55	58.78	0.65	0.67	0.08

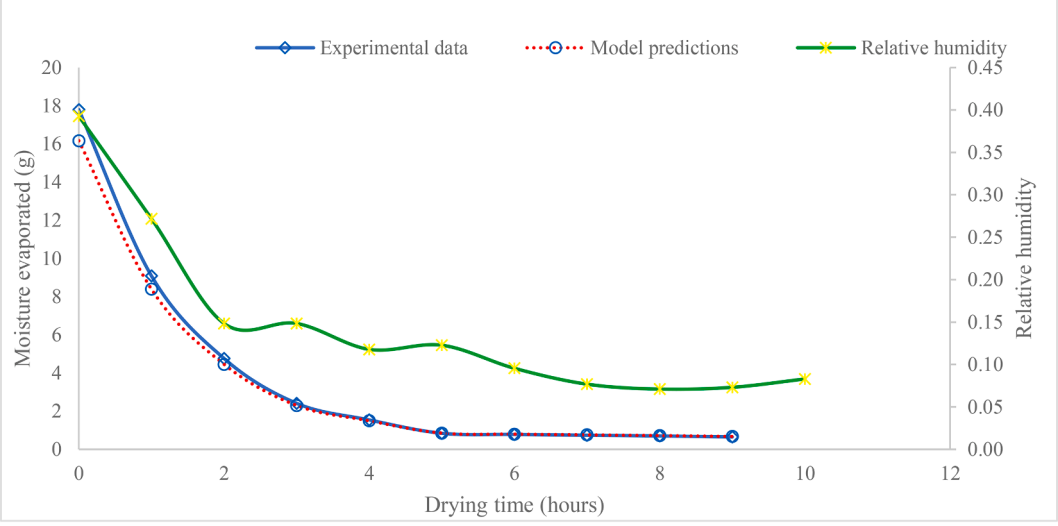

Fig. 12. Moisture evaporated and relative humidity in solar-exhaust gas mode of drying.

3.3. Heat exchanger performance in exhaust gas mode of drying

Comparison of drying time for solar, solar exhaust gas, and exhaust gas modes of drying is illustrated in Fig. 21. The heat exchanger provided the required heat energy to dry black nightshade seeds in 14 h in exhaust gas mode of drying. Referring to Fig. 22 and considering outside and inside temperatures of this mode of drying, the average hourly rise in temperature inside the dryer was 8.04 °C with a minimum rise of 3.7 °C and a maximum of 9.41 °C when exhaust gas was utilized to provide heat energy. Heat energy recovered from exhaust gas of a diesel engine kept the temperatures inside the dryer higher than outside. However, relative humidity inside the dryer were higher than those outside because water vapor from the open cooling system of a diesel engine kept the dryer moist. In a study by Ndirangu *et al.* (2020), the system

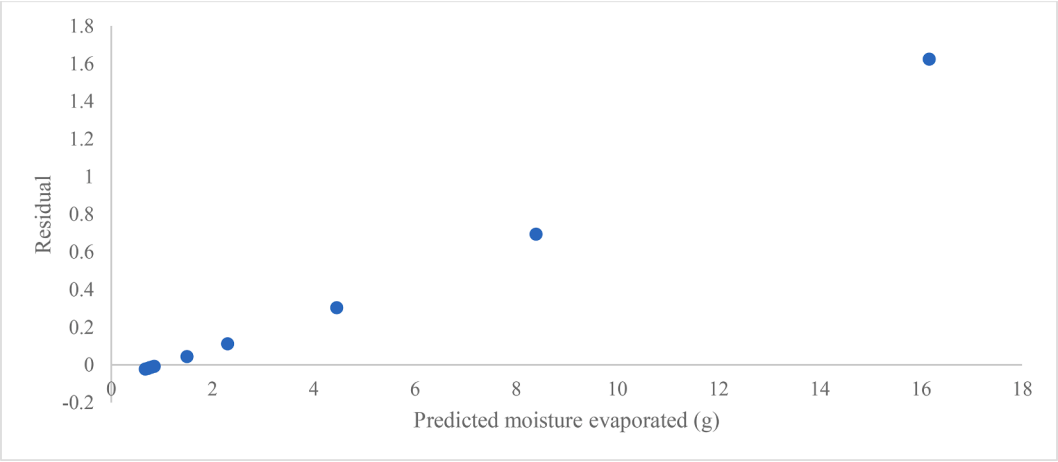

Fig. 13. Residual plots of predicted moisture evaporated in solar-exhaust gas mode of drying.

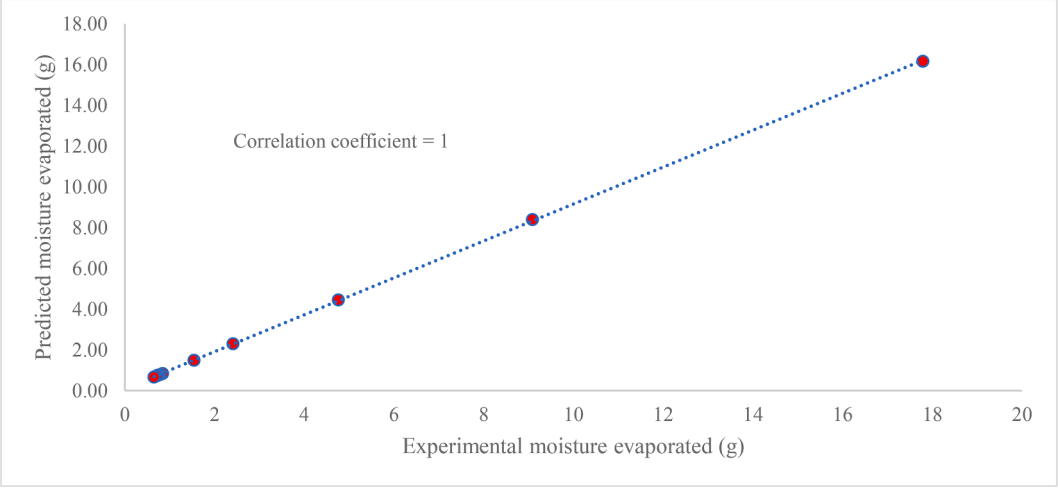

Fig. 14. Correlation between predicted and experimental moisture evaporated in solar-exhaust gas mode of drying.

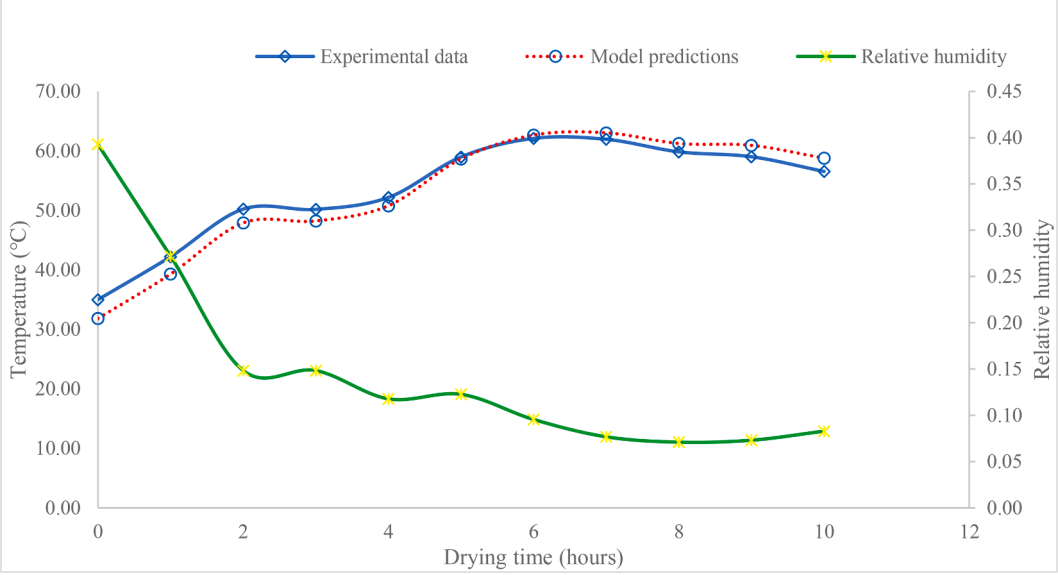

Fig. 15. Black nightshade seeds temperature and relative humidity in solar-exhaust gas mode of drying.

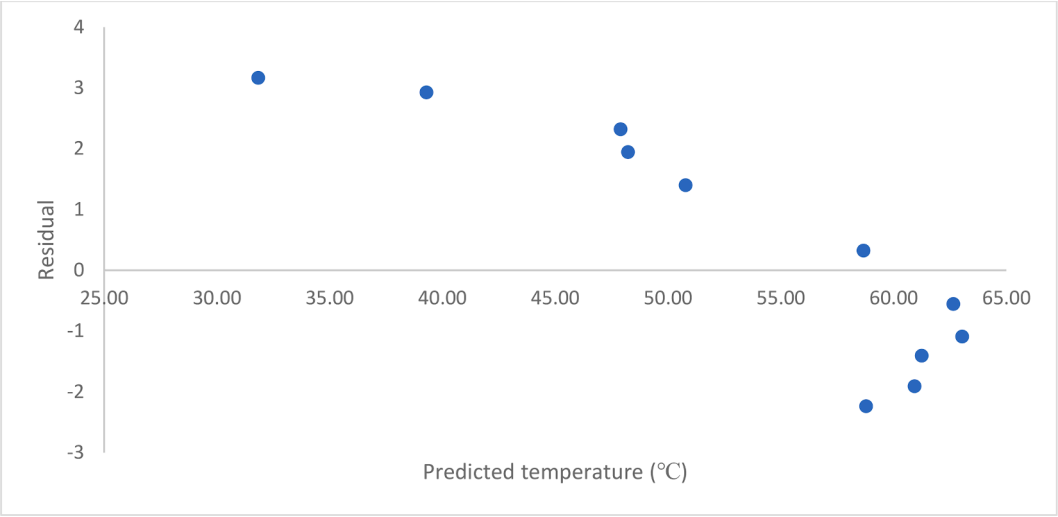

Fig. 16. Residual plots of black night shade seeds predicted temperature in solar-exhaust gas mode of drying.

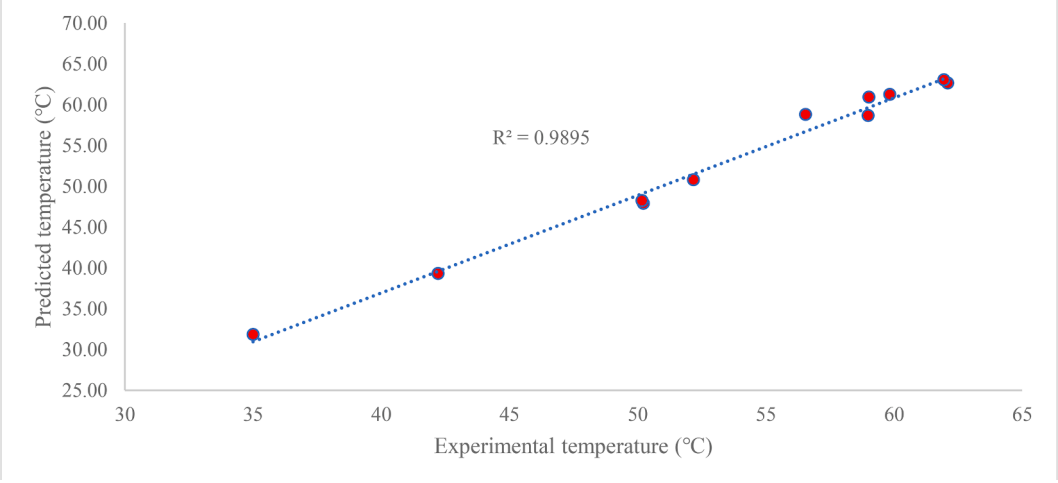

Fig. 17. Correlation between predicted and experimental black night shade seeds temperature in solar-exhaust gas mode of drying.

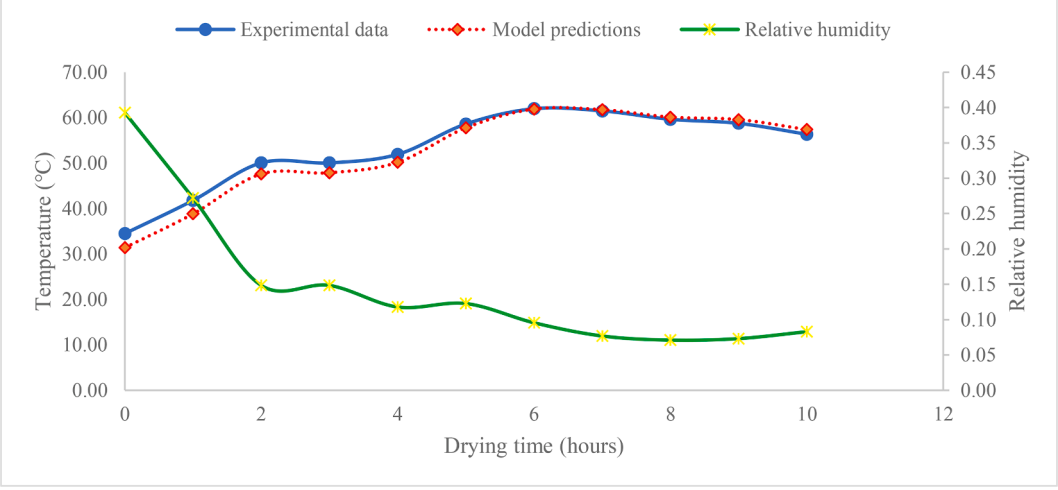

Fig. 18. Greenhouse dryer room air temperature and relative humidity in solar-exhaust gas mode of drying.

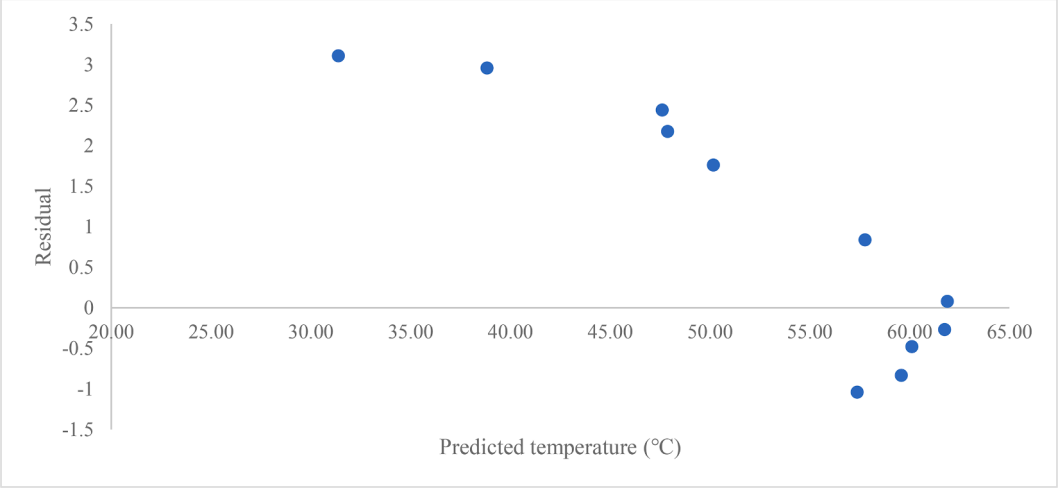

Fig. 19. Residual plots of greenhouse dryer room air predicted temperature in solar-exhaust gas mode of drying.

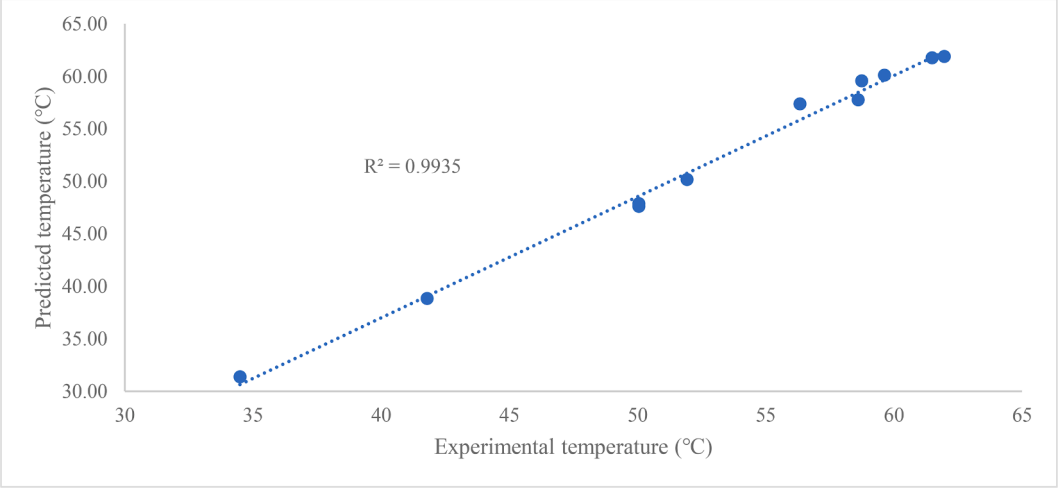

Fig. 20. Correlation between predicted and experimental greenhouse dryer room air temperature in solar-exhaust gas mode of drying.

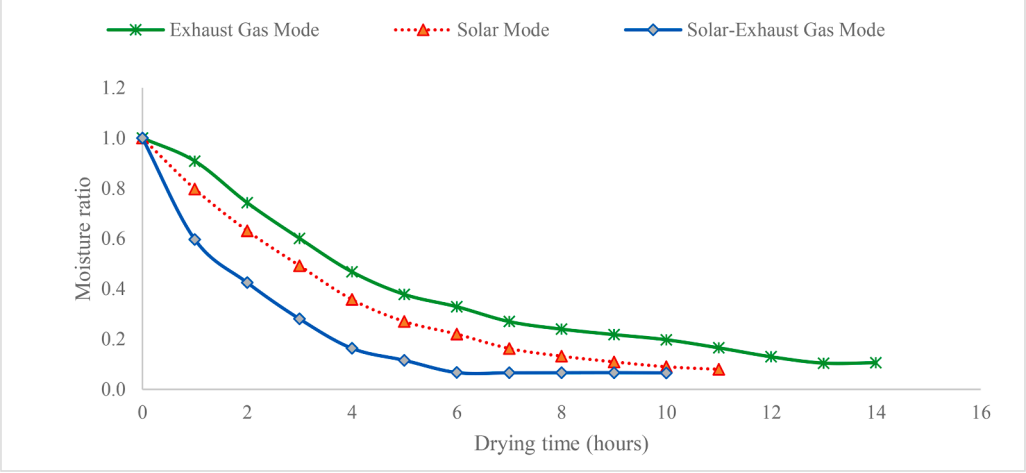

Fig. 21. Drying time comparison for solar, solar-exhaust gas, and exhaust gas modes of drying.

performance of a developed multipurpose solar-biomass greenhouse dryer improved when solar energy was backed up with biomass energy. The drying increased by about 18 to 19% using the solar-biomass mode compared to both natural and forced convection modes. In conclusion, the authors have recommended more tests to be undertaken to fully analyze the dryer's performance, especially in optimizing additional

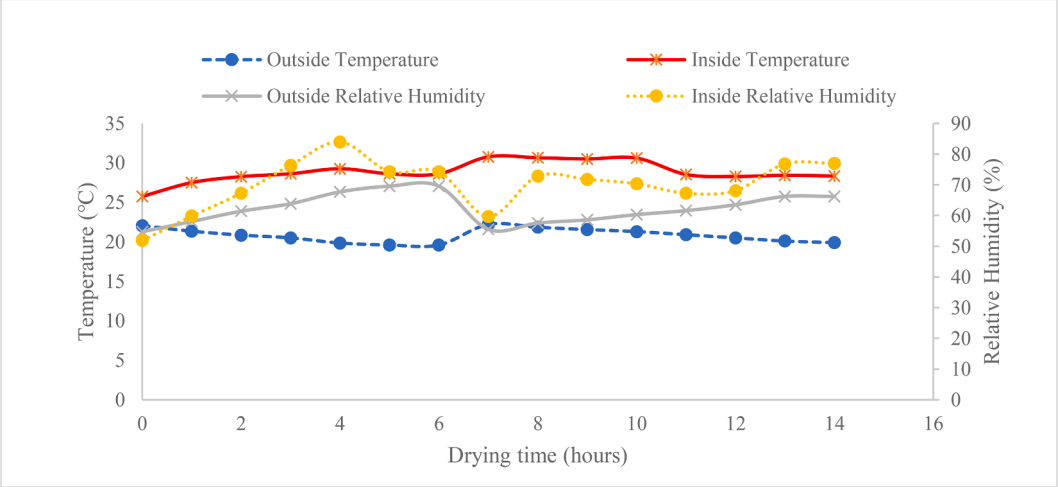

Fig. 22. Relative humidity and temperature variations with drying time in exhaust mode.

Table 8
Experimental and predicted data from forced convection exhaust gas drying mode.

Drying Time (hours)	Experimental T_r (°C)	Predicted T_r (°C)	Experimental T_b (°C)	Predicted T_b (°C)	Experimental m_{ev} (g)	Predicted m_{ev} (g)	γ_v (%)
0	25.75	25.57	25.94	25.20	0	0	0.52
1	27.50	27.44	27.98	27.27	22.33	22.89	0.60
2	28.26	28.27	28.43	27.76	11.00	11.51	0.67
3	28.62	28.68	28.91	28.30	5.80	6.15	0.76
4	29.26	29.39	29.98	29.45	3.19	3.43	0.84
5	28.62	28.74	29.02	28.55	1.93	2.11	0.74
6	28.62	28.78	29.26	28.88	1.30	1.45	0.74
7	30.77	31.13	31.08	30.82	0.86	0.99	0.60
8	30.65	31.04	31.48	31.34	0.63	0.74	0.73
9	30.50	30.93	31.02	30.99	0.48	0.59	0.72
10	30.60	31.09	30.88	30.98	0.37	0.47	0.70
11	28.53	28.92	29.24	29.45	0.27	0.36	0.67
12	28.28	28.72	28.66	29.02	0.19	0.28	0.68
13	28.43	28.94	29.26	29.78	0.14	0.23	0.77
14	28.34	28.91	28.85	29.54	0.13	0.22	0.77

heat energy to achieve desired temperatures.

Table 8 is a summary of experimental and predicted results of changes in evaporated moisture, greenhouse dryer room air temperature, black nightshade seeds temperature, and air relative humidity in exhaust gas mode of drying.

The results of moisture evaporated (experimental and predicted) and relative humidity are plotted in Fig. 23 from which the model's performance based on RMSE was found as 0.2453. The rate of heat utilized

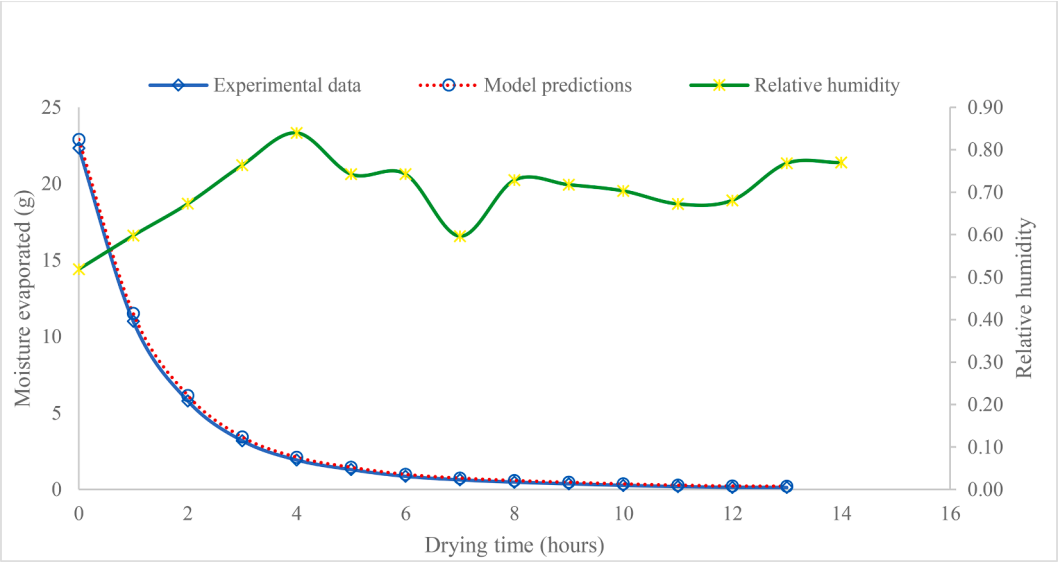

Fig. 23. Moisture evaporated and relative humidity in exhaust gas mode of drying.

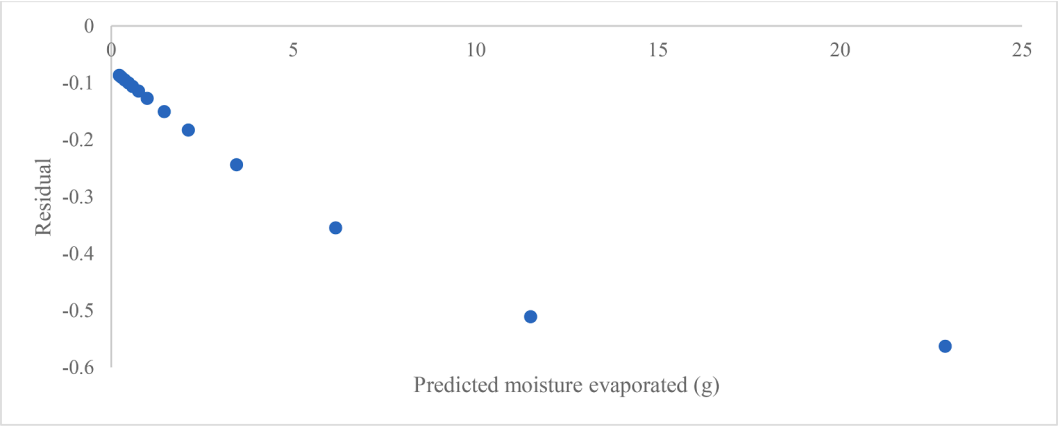

Fig. 24. Residual plots of predicted moisture evaporated in exhaust gas mode of drying.

for exhaust gas mode of drying ranged from 21.69 to 668.11 $J/m^2.s$ and peaked after 8 h of drying when convective heat transfer coefficient was 2.55 W/m^2. °C and evaporative heat transfer coefficient was 18.29 W/m^2. °C. Moisture evaporated and relative humidity decreased with increasing drying time. Residual plots of predicted moisture evaporated are shown in Fig. 24 with all the 15 data points observed as negative. A correlation coefficient of 0.9999 was obtained for predicted versus experimental moisture evaporated shown in Fig. 25. From a two-tailed *t*-test of two samples while assuming equal variances at 0.05 level of significance, experimental moisture evaporated data had a mean of 3.47 g when the predicted had a mean of 3.67 g ($t_{calc} = 0.9333$, $t_{crit} = 2.0556$). Thus, there was enough evidence to retain the null hypotheses that there is no difference in the means between predicted and experimental observations of moisture evaporated and it was concluded with 95% confidence that the model is useful in predicting moisture evaporated from black nightshade seeds. From the iterations performed, the model parameters Ω_0, Ω_1, Ω_2, Ω_3, Ω_4, and Ω_5 were quantified for exhaust gas mode of drying.

The experimental and predicted black nightshade seeds temperatures against drying time are plotted in Fig. 26 from which the results of the model's performance based on RMSE was found as 0.4859. The plot shows that there is an increasing nonlinear relationship between drying time and black nightshade seeds temperature for the first eight hours of drying and thereafter, a decreasing nonlinear relationship is observed for the rest of the drying period. The corresponding residual versus fits plot for the data set with black nightshade seeds temperature as the response and drying time as the predictor is shown in Fig. 27. The residual plots show nonlinearity and an indication of cyclic behavior. Fig. 28. is a goodness of fit plot of the predicted temperatures against experimental observations which show a correlation coefficient of 0.9620. The predicted black nightshade seeds temperature show agreement with experimental observations and from Fig. 27, none of the data points fell directly on the residual equal to zero line. The residuals depart from the zero line in a systematic manner with most of the data points concentrated between 27 and 30 °C and are positive for ten values and negative for five values. From a two-tailed *t*-test of two samples while assuming equal variances at 0.05 level of significance, experimental black nightshade seeds temperature data had a mean of 29.33 °C when the predicted data had a mean of 29.15 °C ($t_{calc} = 0.7537$, $t_{crit} = 2.0484$). Thus, there was enough evidence to retain the null hypotheses that there is no difference in the means between predicted and experimental observations of black nightshade seeds temperatures and it was concluded with 95% confidence that the model is useful in predicting the temperature of the seeds. Model parameters ξ_0, ξ_1, and ξ_2 were quantified to show the main effects of screening and characterizing black nightshade seeds temperature prediction model. The model parameters ξ_3 quantified the interaction (cross product) term between drying time and experimental temperature data, ξ_4 quantified the first leading term with the second degree on drying time factor, ξ_5 quantified the second order term corresponding to black nightshade seeds experimental temperature data and ϖ was the random error term that accounted for experimental error in the system.

Experimental and predicted greenhouse dryer room air temperatures against drying time are plotted in Fig. 29 from which the results of the

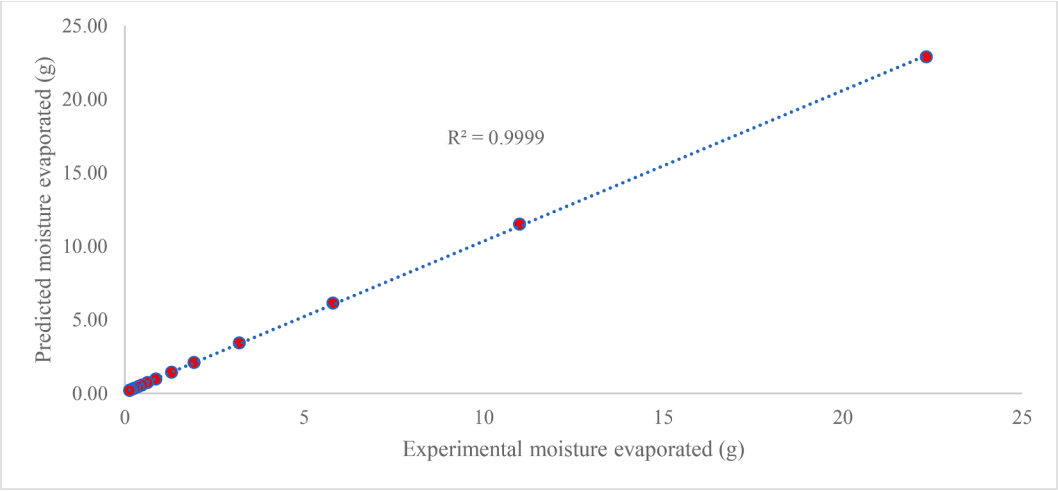

Fig. 25. Correlation between predicted and experimental moisture evaporated in exhaust gas mode of drying.

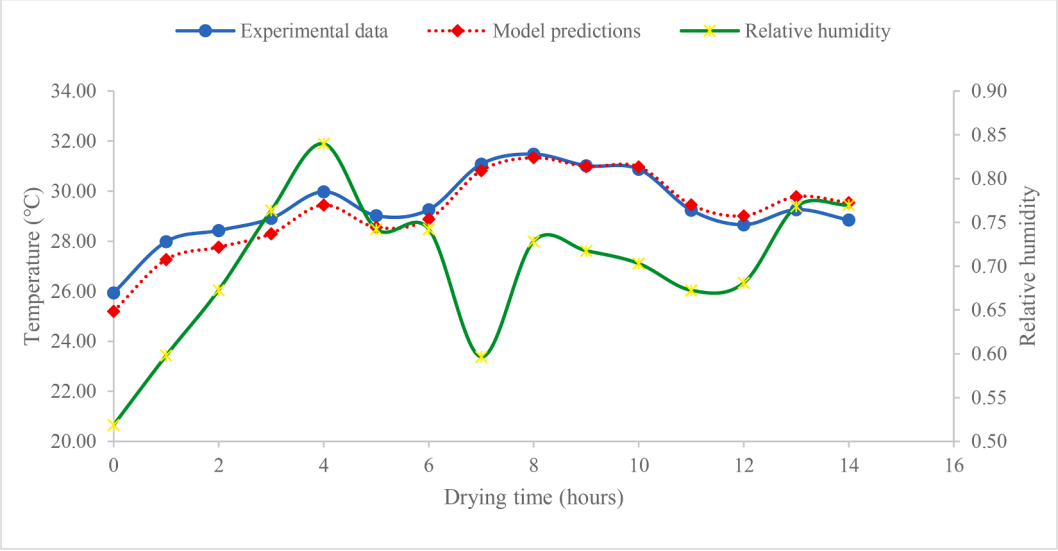

Fig. 26. Black nightshade seeds temperature and relative humidity in exhaust gas mode of drying.

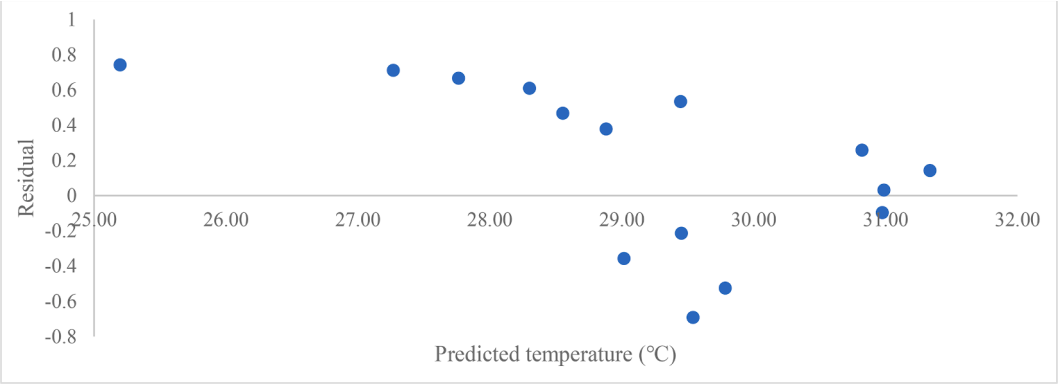

Fig. 27. Residual plots of black night shade seeds predicted temperature in exhaust gas mode of drying.

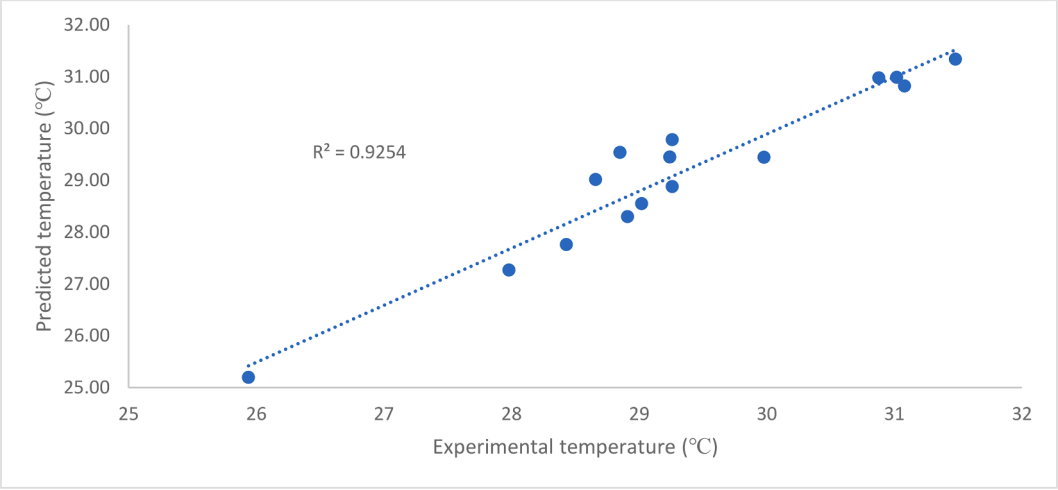

Fig. 28. Correlation between predicted and experimental black night shade seeds temperature in exhaust gas mode of drying.

model's performance based on RMSE was found as 0.3392. The plot shows that there is an increasing nonlinear relationship between drying time and greenhouse dryer room air temperature for the first eight hours of drying and thereafter, a decreasing nonlinear relationship is observed for the rest of the drying period. The corresponding residual plot of greenhouse dryer room air predicted temperature is shown in Fig. 30. The plot show nonlinearity and indication of cyclic behavior. Observations from Fig. 31 show a correlation coefficient of 0.9925. With

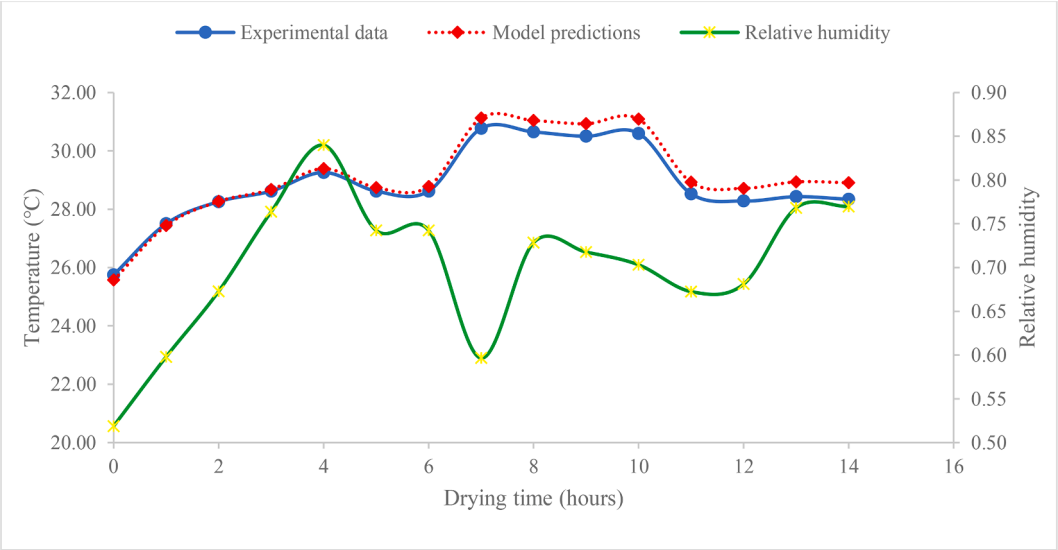

Fig. 29. Greenhouse dryer room air temperature and relative humidity in exhaust gas mode of drying.

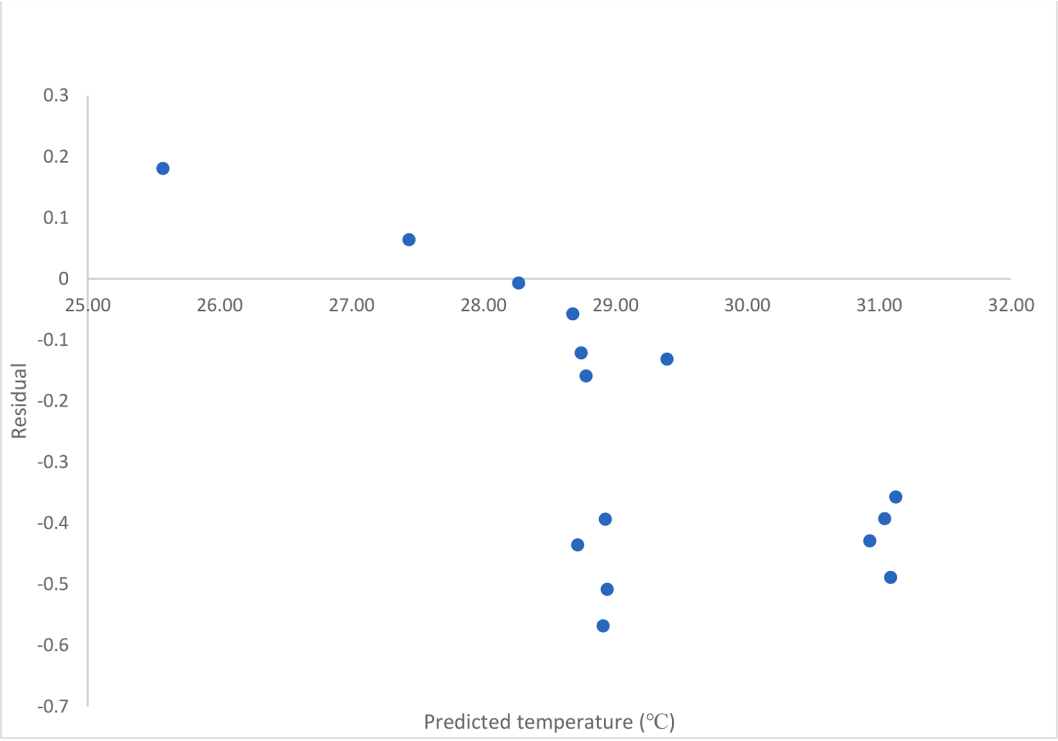

Fig. 30. Residual plots of greenhouse dryer room air predicted temperature in exhaust gas mode of drying.

reference to Fig. 30, none of the data points fell directly on the residual equal to zero line. The residuals depart from the zero line in a systematic manner with most of the data points concentrated between 28 and 31 °C. Two data points are positive while 14 are negative. A two-tailed *t*-test of two samples while assuming equal variances at 0.05 level of significance, show that experimental and predicted greenhouse dryer room air temperature data had means of 28.85 °C and 29.1 °C, respectively (t_{calc} = 0.632, t_{crit} = 2.048). Thus, there was enough evidence to retain the null hypotheses that there is no difference in the means between predicted and experimental observations of greenhouse dryer room air temperatures and it was concluded with 95% confidence that the model is useful in predicting room air temperature of the greenhouse dryer. From iterations, the model parameters ζ_0, ζ_1, and ζ_2 were quantified to show the main effects of screening and characterizing the greenhouse dryer room air temperature prediction model. The model parameters ζ_3 quantified the interaction (cross product) term between drying time and experimental temperature data, ζ_4 quantified the first leading term with the second degree on drying time factor, ζ_5 quantified the second order term corresponding to greenhouse dryer room air experimental temperature and ϱ was the random error term that accounted for the experimental error in the system.

3.4. Summary of models' parameters

A summary of the model parameters estimated from experimental data responses, random error term that accounts for experimental

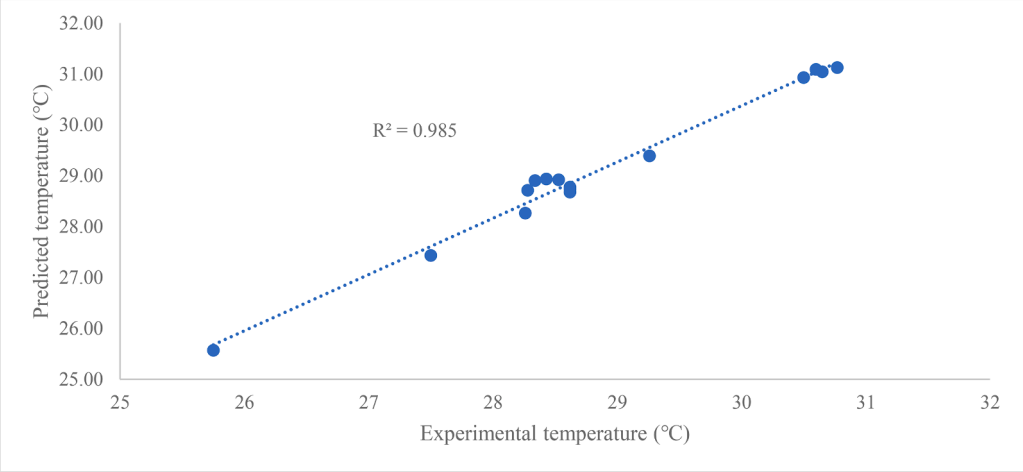

Fig. 31. Correlation between predicted and experimental greenhouse dryer room air temperature in exhaust gas mode of drying.

Table 9
Models, drying modes, RMSE and model parameters.

Model	Solar drying mode	Solar-exhaust gas drying mode	Exhaust gas drying mode
Black nightshade seeds temperature	$RMSE$ = 2.1409	$RMSE$ = 1.9524	$RMSE$ = 0.4859
	$\xi_0 = 0.0495$	$\xi_0 = 0.1424$	$\xi_0 = 0.2382$
	$\xi_1 = 0.0426$	$\xi_1 = 0.0739$	$\xi_1 = 0.0145$
	$\xi_2 = 0.7515$	$\xi_2 = 0.8237$	$\xi_2 = 0.9100$
	$\xi_3 = 0.0002$	$\xi_3 = 0.0046$	$\xi_3 = 0.0005$
	$\xi_4 = 0.0385$	$\xi_4 = 0.0151$	$\xi_4 = 0.0053$
	$\xi_5 = 0.0047$	$\xi_5 = 0.0022$	$\xi_5 = 0.0016$
	$\varpi = 0.0495$	$\varpi = 0.1670$	$\varpi = 0.2433$
Moisture evaporated	$RMSE$ = 0.6455	$RMSE$ = 0.5186	$RMSE$ = 0.2453
	$\Omega_0 = 0.0797$	$\Omega_0 = 0.0699$	$\Omega_0 = 0.0795$
	Ω_1 = 10.1707	$\Omega_1 = 9.7564$	$\Omega_1 = 10.1707$
	$\Omega_2 = 0.9382$	$\Omega_2 = 0.8458$	$\Omega_2 = 0.9382$
	Ω_3 = 331.9957	$\Omega_3 = 328.6183$	$\Omega_3 = 347.7691$
	$\Omega_4 = 0.0382$	$\Omega_4 = 0.0428$	$\Omega_4 = 0.0399$
	$\Omega_5 = 0.0729$	$\Omega_5 = 0.0660$	$\Omega_5 = 0.0761$
Greenhouse dryer room air temperature	$RMSE$ = 2.1257	$RMSE$ = 1.7836	$RMSE$ = 0.3392
	$\zeta_0 = 1.1590$	$\zeta_0 = 0.2070$	$\zeta_0 = 0.2017$
	$\zeta_1 = 0.2880$	$\zeta_1 = 0.0460$	$\zeta_1 = 0.0154$
	$\zeta_2 = 0.8505$	$\zeta_2 = 0.8199$	$\zeta_2 = 0.9079$
	$\zeta_3 = 0.0052$	$\zeta_3 = 0.0030$	$\zeta_3 = 0.0001$
	$\zeta_4 = 0.0158$	$\zeta_4 = 0.0139$	$\zeta_4 = 0.0018$
	$\zeta_5 = 0.0002$	$\zeta_5 = 0.0023$	$\zeta_5 = 0.0028$
	$\varrho = 1.1824$	$\varrho = 0.1552$	$\varrho = 0.1504$

inaccuracies in the system and RMSE that measures the mean difference values predicted by the models and the actual values are given in Table 9.

4. Conclusions

In this paper, a HRHE used for the recovery of diesel engine exhaust gas energy was developed. This energy was used to supplement the heating requirements in a solar-exhaust gas greenhouse dryer for black nightshade seeds. An evaluation of the heat exchanger was done to establish its suitability to meet the seeds drying process. Through computation and analysis of the effectiveness of the heat exchanger, some conclusions are drawn. The maximum thermal energy available in the exhaust gas of the diesel engine was 4.45 kW when the engine was operated at 2500 rpm. The mass flow rate of exhaust gas at this speed is 45.07 kg/h at a temperature of 357.36 °C. Increased engine speed results in increased heat energy in exhaust gas because of an increase in mass flow rate. At higher speeds of 2000 to 2500 rpm mass flow rates of exhaust gas had insignificant effect on temperatures, therefore, there was no significant difference between mass flow rates of exhaust gas for three engine speeds: 2000 rpm, 2250 rpm, and 2500 rpm, ($F_{calc,} = 2.767$, $F_{crit,\ 0.95} = 3.89$, $F_{crit,\ 0.99} = 6.93$ and p-value = 0.103). The heat exchanger raised the dryer temperature by an average of 11.78 °C when temperature differences between inside and outside were compared in solar-exhaust gas mode of drying. The performance of the solar-exhaust gas greenhouse dryer improved when heat energy from exhaust gas was used as a supplement in the drying technique and as a result drying time for black nightshade seeds was significantly reduced from 11 h in solar mode to 10 h in solar-exhaust gas mode of drying. Generally, the drying rate of black nightshade seeds increased with increase in temperature—as observed in solar-exhaust gas drying mode—and decreased with increase in relative humidity—as depicted in exhaust gas drying mode whose experiments were performed when solar radiation was low, and humidity inside the dryer was high due to the presence of water vapor evaporating from the open cooling system of a diesel engine. The rate of heat utilized for solar-exhaust gas mode ranged from 40.49 to 685.94 $J/m^2.s$ and from 21.69 to 668.11 $J/m^2.s$ in exhaust gas mode of drying. The average hourly rise in temperature inside the dryer was 8.04 °C with a minimum rise of 3.7 °C and a maximum of 9.41 °C when exhaust gas was utilized to provide heat energy. The three proposed thermal models for temperatures and moisture evaporation performed better with low RMSEs in exhaust gas mode compared to the other modes of drying. The concept of using a heat exchanger in a solar-exhaust gas dryer was successfully applied in the recovery of exhaust gas energy from a diesel engine—heat energy that under normal circumstances is wastefully released to the environment. Use of diesel engines to power hammer mills in Kenya is known to produce regulated and unregulated emissions which are hazardous to public health. However, the released pollutants contain heat energy in their composition, and it is therefore necessary that further research is done to find solutions capable of recovering the energy for useful work. It was noted that exhaust gas particles adhere to the wall of the heat exchanger, and this may increase thermal resistance over a prolonged period of time.

Conflict of interest and authorship confirmation form

- All authors have participated in the conception, design, analysis, and interpretation of the data; drafting of the article, revising it critically for important intellectual content; and approval of the final version.
- This manuscript has not been submitted to, nor is it under review at, another journal or other publishing venue.

- The authors have no affiliation with any organization with a direct or indirect financial interest in the subject matter discussed in the manuscript.

Declaration of Competing Interest

The authors declare that they have no known competing financial interests or personal relationships that could have appeared to influence the work reported in this paper.

Data Availability

Data will be made available on request.

Acknowledgments

The authors would like to acknowledge the African Development Bank (AfDB) through the Ministry of Education, Science and Technology (MoEST) for the financial support for this work.

References

[1] L.W. Wang, R.Z. Wang, J.Y. Wu, K. Wang, S.G. Wang, Adsorption ice makers for fishing boats driven by the exhaust heat from diesel engine: choice of adsorption pair, Energy Conversion and Manag. 45 (13–14) (2004) 2043–2057.
[2] H. Jouhara, V. Anastasov, I. Khamis, Potential of heat pipe technology in nuclear seawater desalination, Desalination 249 (3) (2009) 1055–1061.
[3] L.W. Wang, C.Z. Liu, L. Jiang, Y.J. Zhao, R.Z. Wang, Performance of a resorption cycle for recovering the waste heat from vehicles, Sci. Technol. Built Environ. 21 (3) (2015) 280–289.
[4] H. Jouhara, R. Meskimmon, Heat pipe based thermal management systems for energy-efficient data centres, Energy 77 (2014) 265–270.
[5] S. Popli, P. Rodgers, V. Eveloy, Trigeneration scheme for energy efficiency enhancement in a natural gas processing plant through turbine exhaust gas waste heat utilization, Appl. Energy 93 (2012) 624–636.
[6] ... & H. Jouhara, S. Almahmoud, A. Chauhan, B. Delpech, G. Bianchi, S.A. Tassou, J.J. Arribas, Experimental and theoretical investigation of a flat heat pipe heat exchanger for waste heat recovery in the steel industry, Energy 141 (2017) 1928–1939.
[7] A.M. Alklaibi, Utilization of exhaust gases heat from gas turbine with air bottoming combined cycle, Energy 133 (2017) 1108–1120.
[8] ... & H. Jouhara, D. Bertrand, B. Axcell, L. Montorsi, M. Venturelli, S. Almahmoud, A. Chauhan, Investigation on a full-scale heat pipe heat exchanger in the ceramics industry for waste heat recovery, Energy 223 (2021), 120037.
[9] H. Jouhara, A. Chauhan, T. Nannou, S. Almahmoud, B. Delpech, L.C. Wrobel, Heat pipe based systems-advances and applications, Energy 128 (2017) 729–754.
[10] J.P. Liu, J.Q. Fu, C.Q. Ren, L.J. Wang, Z.X. Xu, B.L. Deng, Comparison and analysis of engine exhaust gas energy recovery potential through various bottom cycles, Appl. Therm. Eng. 50 (1) (2013) 1219–1234.
[11] H. Jouhara, N. Khordehgah, S. Almahmoud, B. Delpech, A. Chauhan, S.A. Tassou, Waste heat recovery technologies and applications, Therm. Sci. Eng. Progress 6 (2018) 268–289.
[12] T. Wilberforce, I. Muhammad, Dynamic modelling and analysis of organic rankine cycle power units for the recovery of waste heat from 110kW proton exchange membrane fuel cell system, Int. J. Thermofluids (2023), 100280.
[13] M. Mahmoud, S. Naher, M. Ramadan, M.A. Abdelkareem, H. Jaber, A.G. Olabi, Investigation of a ground-cooled organic Rankine cycle for waste heat recovery, Int. J. Thermofluids 18 (2023), 100348.
[14] H. Jouhara, A.G. Olabi, Industrial waste heat recovery, Energy 160 (2018) 1–2.
[15] Z. Zhang, H. Liu, Z. Yue, Y. Wu, X. Kong, Z. Zheng, M. Yao, Effects of multiple injection strategies on heavy-duty diesel energy distributions and emissions under high peak combustion pressures, Front. Energy Res. (2022) 430.
[16] Z. Zheng, M. Xia, H. Liu, X. Wang, M. Yao, Experimental study on combustion and emissions of dual fuel RCCI mode fueled with biodiesel/n-butanol, biodiesel/2, 5-dimethylfuran and biodiesel/ethanol, Energy 148 (2018) 824–838.
[17] ... & Z. Zhang, H. Liu, Z. Yue, Y. Li, H. Liang, X. Kong, M. Yao, Effects of intake high-pressure compressed air on thermal-work conversion in a stationary diesel engine, Int. J. Green Energy 20 (3) (2023) 338–351.
[18] Z. Zheng, L. Yue, H. Liu, Y. Zhu, X. Zhong, M. Yao, Effect of two-stage injection on combustion and emissions under high EGR rate on a diesel engine by fueling blends of diesel/gasoline, diesel/n-butanol, diesel/gasoline/n-butanol and pure diesel, Energy Conversion and Manag. 90 (2015) 1–11.
[19] M.V. De Poures, D. Damodharan, K. Gopal, V.C. Augustin, M.R. Swaminathan, Prediction of emissions and performance of a diesel engine fueled with waste cooking oil and C8 oxygenate blends using response surface methodology, J. Clean. Prod. (2022), 133323.
[20] M. Pan, Z. Zheng, R. Huang, X. Zhou, H. Huang, J. Pan, Z. Chen, Reduction in PM and NOX of a diesel engine integrated with n-octanol fuel addition and exhaust gas recirculation, Energy 187 (2019), 115946.
[21] H.A. Dhahad, M.T. Chaichan, T. Megaritis, Performance, regulated and unregulated exhaust emission of a stationary compression ignition engine fueled by water-ULSD emulsion, Energy 181 (2019) 1036–1050.
[22] M.T. Chaichan, Combustion and emission characteristics of E85 and diesel blend in conventional diesel engine operating in PPCI mode, Therm. Sci. Eng. Progress 7 (2018) 45–53.
[23] H. De Groote, S.C. Kimenju, Comparing consumer preferences for color and nutritional quality in maize: application of a semi-double-bound logistic model on urban consumers in Kenya, Food Policy 33 (4) (2008) 362–370.
[24] J.S. Jadhao, D.G. Thombare, Review on exhaust gas heat recovery for IC engine, Int. J. Eng. Innovative Technol. 2 (12) (2013) 93–100.
[25] E. Tavousi, N. Perera, D. Flynn, R. Hasan, Heat transfer and fluid flow characteristics of the passive method in double tube heat exchangers: a critical review, Int. J. Thermofluids (2023), 100282.
[26] H. Jouhara, H. Ezzuddin, Thermal performance characteristics of a wraparound loop heat pipe (WLHP) charged with R134A, Energy 61 (2013) 128–138.
[27] O.M. Adesusi, O.R. Adetunji, S.I. Kuye, A.I. Musa, T.J. Erinle, O.B. Gbadamosi-Olatunde, S.O. Ipadeola, A comprehensive review of the materials degradation phenomena in solid-liquid phase change materials for thermal energy storage, Int. J. Thermofluids (2023), 100360.
[28] M. Tawalbeh, H.A. Khan, A. Al-Othman, F. Almomani, S. Ajith, A comprehensive review on the recent advances in materials for thermal energy storage applications, Int. J. Thermofluids (2023), 100326.
[29] M.I. Alamayreh, A. Alahmer, Design a solar harvester system capturing light and thermal energy coupled with a novel direct thermal energy storage and nanoparticles, Int. J. Thermofluids 18 (2023), 100328.
[30] H. Jouhara, A. Żabnieńska-Góra, N. Khordehgah, D. Ahmad, T. Lipinski, Latent thermal energy storage technologies and applications: a review, Int. J. Thermofluids 5 (2020), 100039.
[31] ... & M.M. Hathal, T. Al-Jadir, F. Al-Sheikh, M.S. Edan, M.J. Haider, R.A. Rsool, T. Badawy, Thermal performance characterization of a thermal energy storage tank with various phase change materials, Int. J. Thermofluids 18 (2023), 100322.
[32] R. Murr, G. El Achkar, J. Faraj, H. El Hage, C. Castelain, M. Khaled, Using solar air heating for fruit drying: thermo-economic and environmental studies, Int. J. Thermofluids 18 (2023), 100366.
[33] F.G. Kiburi, C.L. Kanali, G.M. Kituu, P.O. Ajwang, E.K. Ronoh, Performance evaluation and economic feasibility of a solar-biomass hybrid greenhouse dryer for drying Banana slices, Renew. Energy Focus 34 (2020) 60–68.
[34] C. Kanali, G. Kituu, U. Mutwiwa, J. Mung'atu, E. Ronoh, S. Njuguna, L. Mulamu, RE4Food Project Report, Jomo Kenyatta University of Agriculture and Technology (JKUAT), Kenya, 2017.
[35] S.N. Ndirangu, E.K. Ronoh, C.L. Kanali, U.N. Mutwiwa, G.M. Kituu, Design and performance evaluation of an improved solar-biomass greenhouse dryer for drying selected crops in Western Kenya, Agricultural Eng. Int.: CIGR J. 22 (3) (2020) 219–229.
[36] N. Chowdhury, A. Ghosh, G. Chandra, Mosquito Larvicidal activities of solanum Villosum berry extract against the dengue vector Stegomyia Aegypti, BMC Complement. Altern. Med. 8 (1) (2008) 1–8.
[37] R.H. Perry, D.W. Green, Perry's Chemical Engineers' Handbook, 7th edition, McGraw-Hill, New York, 1997.
[38] B.E. Rapp, Microfluidics: Modeling, Mechanics, and Mathematics, William Andrew, 2016.
[39] E.S. Menon, Transmission Pipeline Calculations and Simulations Manual, Gulf Professional Publishing, 2014.
[40] P. Sawant, M. Warstler, S. Bari, Exhaust tuning of an internal combustion engine by the combined effects of variable exhaust pipe diameter and an exhaust valve timing system, Energies 11 (6) (2018) 1545.
[41] U. Kesgin, Study on the design of inlet and exhaust system of a stationary internal combustion engine, Energy Conversion and Manag. 46 (13–14) (2005) 2258–2287.
[42] R Core Team, R: A Language and Environment for Statistical Computing, R Foundation for Statistical Computing, Vienna, Austria, 2023. https://www.R-project.org/.
[43] P.S. Chauhan, A. Kumar, Performance analysis of greenhouse dryer by using insulated north-wall under natural convection mode, Energy Reports 2 (2016) 107–116.
[44] S.I. Anwar, G.N. Tiwari, Convective heat transfer coefficient of crops in forced convection drying — An experimental study, Energy Conversion and Manag. 42 (14) (2001) 1687–1698.
[45] L.W. Wang, R.Z. Wang, Z.S. Lu, C.J. Chen, Studies on split heat pipe type adsorption ice-making test unit for fishing boats: choice of heat pipe medium and experiments under unsteady heating sources, Energy Conversion and Manag. 47 (15–16) (2006) 2081–2091.
[46] L.W. Wang, R.Z. Wang, J.Y. Wu, Y.X. Xu, S.G. Wang, Design, simulation and performance of a waste heat driven adsorption ice maker for fishing boat, Energy 31 (2–3) (2006) 244–259.
[47] P. Kosky, R.T. Balmer, W.D. Keat, G. Wise, Exploring Engineering: an Introduction to Engineering and Design, Academic Press, 2015.
[48] ... & H. Jouhara, S. Almahmoud, D. Brough, V. Guichet, B. Delpech, A. Chauhan, N. Serey, Experimental and theoretical investigation of the performance of an air to water multi-pass heat pipe-based heat exchanger, Energy 219 (2021), 119624.
[49] P. Lad, R. Kumar, R. Saxena, J. Patel, Numerical investigation of phase change material assisted indirect solar dryer for food quality preservation, Int. J. Thermofluids 18 (2023), 100305.